# 3D crustal stress state of Western Central Europe according to a data-calibrated geomechanical model - first results

Steffen Ahlers[1], Andreas Henk[1], Tobias Hergert[1], Karsten Reiter[1], Birgit Müller[2], Luisa Röckel[2], Oliver Heidbach[3], Sophia Morawietz[3], Magdalena Scheck-Wenderoth[3], Denis Anikiev[3]

5   [1] Institut für Angewandte Geowissenschaften, TU Darmstadt, 64287 Darmstadt, Germany
[2] Institut für Angewandte Geowissenschaften, KIT, 76131 Karlsruhe, Germany
[3] Deutsches GeoForschungsZentrum (GFZ), 14473 Potsdam, Germany

*Correspondence to*: Steffen Ahlers (ahlers@geo.tu-darmstadt.de)

**Abstract.** The contemporary stress state in the upper crust is of great interest for geotechnical applications and basic
10 research likewise. However, our knowledge of the crustal stress field from the data perspective is limited. For Western
Central Europe basically two datasets are available: Orientations of the maximum horizontal stress ($S_{Hmax}$) and the stress
regime as part of the World Stress Map (WSM) database (Heidbach et al., 2018) as well as a complementary compilation of
stress magnitude data of Germany and adjacent regions (Morawietz et al., 2020). However, these datasets only provide
pointwise, incomplete and heterogeneous information of the 3D stress tensor. Here, we present a geomechanical-numerical
15 model that provides a continuous description of the contemporary 3D crustal stress state on a regional scale for Western
Central Europe. The model covers an area of about 1000 x 1250 km$^2$ and extends to a depth of 100 km containing seven
lithostratigraphic units, with specific material properties (density and elastic rock properties) and laterally varying
thicknesses: A sedimentary unit, four different units of the upper crust, the lower crust and the lithospheric mantle. The
model is calibrated by the two datasets to achieve a best-fit regarding the $S_{Hmax}$ orientations and the minimum horizontal
20 stress magnitudes ($S_{hmin}$). The modelled orientations of $S_{Hmax}$ are almost entirely within the uncertainties of the WSM data
used and the $S_{hmin}$ magnitudes fit to various datasets well. Only the $S_{Hmax}$ magnitudes show locally significant deviations,
primarily indicating too low values in the lower part of the model. The model is open for further refinements regarding
model geometry, e.g., additional layers with laterally varying material properties, and incorporation of future stress
measurements. In addition, it can provide the initial stress state for local geomechanical models with a higher resolution.

## 1 Introduction

Knowledge about the stress state in the upper crust is of great importance for many economic and scientific questions. For
example, wellbore stability (Bell, 2003; Kristiansen, 2004), operation and stimulation of hydrocarbon and geothermal
reservoirs (Altmann et al., 2014; Azzola et al., 2019; Henk, 2009; Smart et al., 2014), slip and dilation tendency of existing
30 faults and fractures (Hettema, 2020; Konstantinovskaya et al., 2012), underground mining (Brady & Brown, 2004) or deep
tunnelling (Diederichs et al., 2004). Furthermore, it plays a decisive role in the search for a disposal site for high-level
radioactive waste, since it is crucial for the short and long-term safety of a possible repository. For all these applications the
contemporary stress state is a key parameter and thus, the quantification of the complete 3D stress tensor is essential.
However, from the data perspective, our knowledge of the stress state in Western Central Europe is limited in particular
35 regarding stress magnitudes information. Public stress information is provided by the World Stress Map (WSM) project
which supplies a global database of the orientation of maximum horizontal stress ($S_{Hmax}$) and the stress regime (Heidbach et
al., 2018) and by a compilation of stress magnitude data for Germany and adjacent regions of Morawietz et al. (2020).
However, these two datasets contain only pointwise information, which is incomplete as only a subset of the stress tensor
components is provided and their spatial distribution is sparse and irregular (Fig. 1a).

40 To provide a continuous description of the 3D stress tensor in the upper crust on a regional scale, we develop in this study the first 3D geomechanical model covering Western Central Europe (Fig. 1). Our model comprises seven lithostratigraphic units, with specific material properties and laterally varying thicknesses: A sedimentary unit, four different units of the upper crust, the lower crust and the lithospheric mantle. The finite element method (FEM) is used to solve the partial differential equation which describes the equilibrium of body and surface forces within an inhomogeneous medium. Our input

45 parameters are density and elastic material properties (Young's modulus and Poisson's ratio). The model is calibrated using appropriate initial conditions and displacement boundary conditions to find a best-fit with respect to the stress orientation and magnitude datasets described above.

## 2 Fundamentals and state of the art

### 2.1 Geology of the study area

50 The crustal and lithospheric structure in the model domain reflects the complex geodynamic evolution of Central Europe since Precambrian times (McCann, 2008; Meschede and Warr, 2019) (Fig. 1b and c). The north-eastern part of the study area belongs to the cratonic unit of Baltica and, more specifically, the East European Craton. This unit consists mainly of high-grade magmatic and metamorphic rocks of Precambrian and early Palaeozoic age. Crustal thickness in the area is about 50 km and a thick mantle lithosphere down to depths of 200 km has been observed. The East European Craton is separated from

55 the Avalonia microplate to the south-west by the Tornquist-Teisseyre Zone and the Thor Suture, respectively (e.g., Maystrenko et al., 2008 and various references therein). At this boundary, a sharp transition to the significantly smaller crustal and lithospheric thicknesses typical for Paleozoic and Mesozoic Europe can be observed (Ziegler and Dèzes, 2006). Western Baltica and eastern Avalonia got into contact during closure of the Tornquist Ocean during Ordovician to Silurian times and the Caledonian orogeny, respectively. At this stage, Laurussia (composed of Laurentia, Baltica and Avalonia) was

60 formed, whose continental crust makes up the northern and eastern part of the study area.

The central part of the model domain comprises the southern part of Avalonia as well as Amorica – microplates and terrane assemblages - which collided during the Variscan orogeny in Late Palaeozoic times (Franke, 1989, 2006; Meschede and Warr, 2019). The low-grade metamorphic rocks of the Rhenohercynian Zone (sensu Kossmat, 1927) represent passive margin sediments which were deposited on thinned crust of south-eastern Avalonia. South-eastward directed subduction and

65 closure of the Rheic Ocean led to the formation of an active margin at the northern rim of Amorica, which nowadays comprises the medium-grade metamorphic and magmatic rocks of the so-called Mid German Crystalline High (Oncken, 1997). Further to the south, the Saxothuringian and Moldanubian Zone represent the remnants of the internal zone of the Variscan orogen with medium- to high-grade metamorphic rocks and abundant granitoids presently exposed at surface. Crustal thickness in this part of the model domain and outside the areas affected by Cenozoic rifting and mountain building

70 is typically in the order of 30 km (Ziegler and Dèzes, 2006).

The southernmost parts of the study area are located in the so-called ALCAPA (Alps–Carpathians–Pannonian) unit or terrane (e.g., Brückl et al., 2010; Schmid et al., 2004). Its geodynamic evolution is closely related to the Alpine orogeny, which lasts since Cretaceous times and is still continuing today.
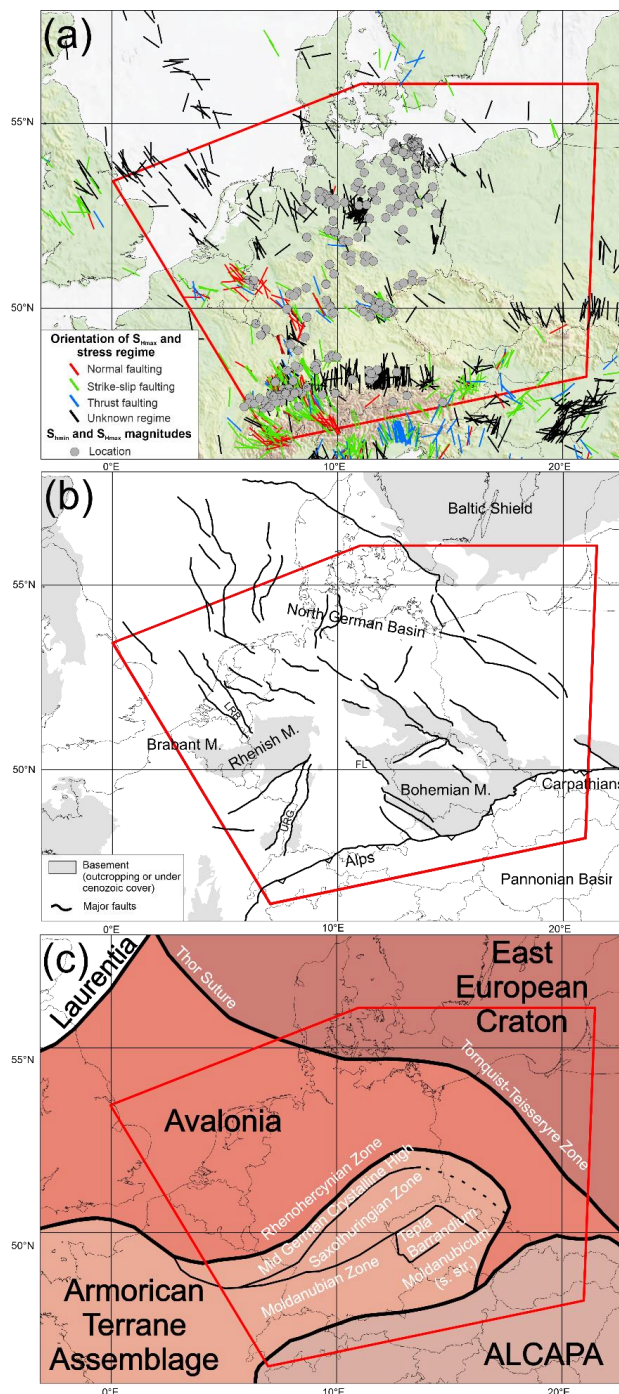
**Figure 1: Maps of Western Central Europe, the red polygon indicates the model area. (a) Topography and overview of calibration data used. Color-coded lines indicate the orientation of S$_{Hmax}$ and the stress regime of the WSM (Heidbach et al., 2018) and additional data of Levi et al. (2019). Grey dots show the positions of stress magnitude data of Morawietz et al. (2020). The topography is based on Smith and Sandwell (1997). (b) Tectonic framework of the model area based on Asch (2005) and Kley and Voigt (2008). FL - Franconian Line, LRB - Lower Rhine Basin, M. - Massif, URG - Upper Rhine Graben. (c) Overview of the crustal units in Central Europe (modified after Kroner et al., 2010). Black titles show tectonic units and white titles sutures and Variscan units.**

### 2.2 Basics of the crustal stress state

The stress state at a given point can be described by a second rank tensor (Fig. 2a) with Pascal ($1\ Pa = N\ m^{-2}$) as the basic unit. Due to its symmetry properties, only six out of nine components are independent from each other (e.g. Jaeger et al., 2011). In the principal axis system, the off-diagonal components vanish and the remaining three components are the principal stresses $\sigma_1$, $\sigma_2$ and $\sigma_3$. Their orientations and magnitudes describe the absolute stress state (Fig. 2b). Assuming that the vertical stress ($S_V$) is one of the three principal stresses (Fig. 2c), the orientation of this so-called reduced stress tensor is determined by the orientation of $S_{Hmax}$. Given that $S_V$ can be approximated by depth and density of the overburden, the remaining unknowns are the magnitudes of $S_{Hmax}$ and the minimum horizontal stress ($S_{hmin}$).
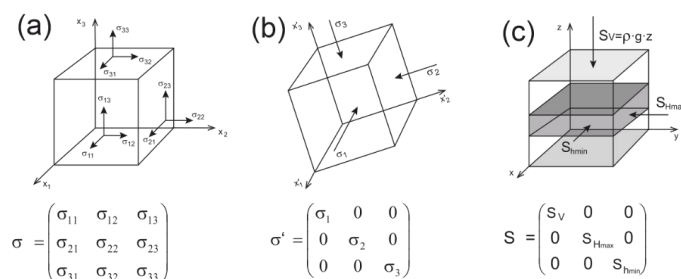
**Figure 2: (a) The nine components of the stress tensor define the stress state at an arbitrary point and enable to compute the stress vector on any surface through that point. To describe the stress tensor components an infinitely small cube with uniform surfaces is used. (b) Due to the conservation of momentum, the stress tensor is symmetric and thus a coordinate system exists where shear stresses vanish along the faces of the cube. In this principal axis system, the remaining three stresses are the principal stresses. (c) Assuming that the vertical stress (the overburden) in the Earth crust $S_V = g \cdot \rho \cdot z$ is a principal stress (g is gravitational acceleration, $\rho$ is the rock density, z is depth), the two horizontal stresses $S_{hmin}$ and $S_{Hmax}$, the minimum and maximum horizontal stress, respectively, are principal stresses as well. This so-called reduced stress tensor is fully determined with four components: The $S_{Hmax}$ orientation and the magnitudes of $S_V$, $S_{hmin}$ and $S_{Hmax}$.**

### 2.3 Data compilation of stress tensor components

The orientation of the stress tensor in the Earth's crust is provided by the WSM database, which is a global compilation providing data on the $S_{Hmax}$ orientation and the stress regime (Heidbach et al., 2018). This stress information is derived from a variety of methods, primarily earthquake focal mechanism solutions, borehole breakouts and drilling-induced tensile fractures (from borehole image or multi-arm caliper log data), in-situ stress measurements (overcoring or hydraulic fracturing) and geologic indicators, such as fault slip and volcanic vent alignment (Amadei and Stephansson, 1997; Ljunggren et al., 2003; Schmitt et al., 2012). The stress information in the WSM database is compiled in a standardized format and quality-ranked for reliability and comparability on a global scale (Heidbach et al., 2010; Zoback, 1992). For Germany and adjacent regions, the $S_{Hmax}$ orientations have been re-evaluated recently (Reiter et al., 2016; Reiter et al., 2015). The new data have been integrated in the latest WSM database release (Heidbach et al., 2018). For stress magnitude data, Morawietz et al. (2020) published a publicly accessible database with 568 data records including a quality assessment of the data for Germany and adjacent regions. These two datasets, the $S_{Hmax}$ orientation of the WSM with some additional data of Levi et al. (2019) and the stress magnitude database are used to calibrate the geomechanical model (Fig. 1a).

### 2.4 Previous models

Modelling the contemporary crustal stress in Western Central Europe has been addressed by various authors since the mid-80s. However, except the model of Buchmann and Connolly (2007) which provide a 3D model of the broader Upper Rhine Graben (URG), all models are 2D and with a strong emphasis on the $S_{Hmax}$ orientation and little regarding the stress magnitudes. Table 1 gives a short overview of their key technical characteristics. If several model versions are published by one author, the most current one is listed. In general, different plastic and elastic material properties with a wide range have

been tested so far and also various boundary conditions have been applied. For a detailed overview we refer to Cacace
120 (2008) and Jarosiński et al. (2006).

The results indicate different main factors influencing the contemporary stress state. The majority of the studies have found
lateral stiffness contrasts in the lithosphere, such as the Bohemian Massif, the Elbe Fault Zone or the Tornquist-Teisseyre
Zone (Cacace, 2008; Grünthal and Stromeyer, 1994; Jarosiński et al., 2006; Marotta et al., 2002) and isostatic effects (Bada
et al., 2001; Kaiser et al., 2005; Jarosiński et al., 2006) to be the main cause of stress perturbations. In addition, faults or fault
125 zones are held responsible for local variation or second-order stresses, respectively (Jarosiński et al., 2006; Kaiser et al.,
2005). An indirect influence of the depth position of the asthenosphere lithosphere boundary (LAB) and the resulting
temperature contrasts and changed mechanical properties are described by Cacace (2008).

**Table 1: Overview of regional scale stress models within the model area**

| Author | Model area | Model dimension | Material law | | Boundary and initial conditions | | Variations | | | |
|---|---|---|---|---|---|---|---|---|---|---|
| | | | elastic | plastic | plate boundary forces | gravity induced forces | density | friction coefficient (faults) | thickness | plastic or elastic material parameters |
| Andeweg, 2002 | European part of Eurasia | 2D | X | | | X | X | | X | |
| Bada et al., 2001 | Pannonian Basin and surrounding orogens | 2D | X | | X | | | | | X |
| Buchmann and Connolly, 2007 | Upper Rhine Graben | 3D | X | X | (x) | | X | | | X |
| Cacace, 2008 | Central European Basin System | 2D, thin sheet | | X | X | | | | | X |
| Goelke and Coblentz, 1996 | European part of Eurasia | 2D | X | | X | | X | | | |
| Grünthal and Stromeyer, 1994 | East and Central Eurasia | 2D | X | | X | | | | | X |
| Jarosiński et al., 2006 | East and Central Europe | 2D | X | | | X | | X | | X |
| Kaiser et al., 2005 | North Germany and South Scandinavia | 2D, thin plate | | X | X | X | | X | | X |
| Marotta et al., 2002 | Germany | 2D, thin sheet | | X | X | | | | X | X |

130 **3. Model setup**

**3.1 Conceptual modelling approach**

To model the contemporary 3D stress field of the upper crust we assume linear elasticity and neglect thermal stresses and
pore pressure effects. With these assumptions, the partial differential equation of the equilibrium of forces has to be solved
(Jaeger et al., 2007). The two contributing forces are volume forces from gravitational acceleration and surfaces forces that
135 are mainly attributed to plate tectonics. The latter are key drivers for the tectonic stress that we observe and they are
parametrized with displacement boundary conditions that are chosen in a way that the resulting stresses deliver a best-fit
with respect to the model-independent stress data. This process is called model calibration which can also be used to estimate
model uncertainties by means of standard deviation (Ziegler et al., 2016; Ziegler and Heidbach, 2020). The technical
procedure is presented in Fig. 3 with a schematic general workflow. The individual text boxes are color-coded indicating the
140 four major steps.

The model geometry reflects the contemporary distribution of rock properties such as density and stiffness and Poisson's ratio. An appropriate initial stresses equilibrates the gravitational stresses and resembles a reference stress state (Fischer and Henk, 2013; Hergert et al., 2015; Reiter and Heidbach, 2014). The orientations of the lateral model boundaries where the displacement boundary conditions are applied are chosen in such a way that the observed $S_{Hmax}$ orientation is perpendicular

145    or parallel to them (Fig. 1a).

For the solution of the partial differential equation of the equilibrium of forces, we use the FEM to estimate an approximated numerical solution. The FEM is appropriate as it allows discretizing complex geometries with unstructured meshes. The commercial FEM software package Abaqus™ v2019 is used. For post-processing we are using Tecplot 360™ enhanced with the GeoStress add-on (Stromeyer and Heidbach, 2017). For the construction and discretization of the 3D model geometry

150    GOCAD™ and HyperMesh™ are used.
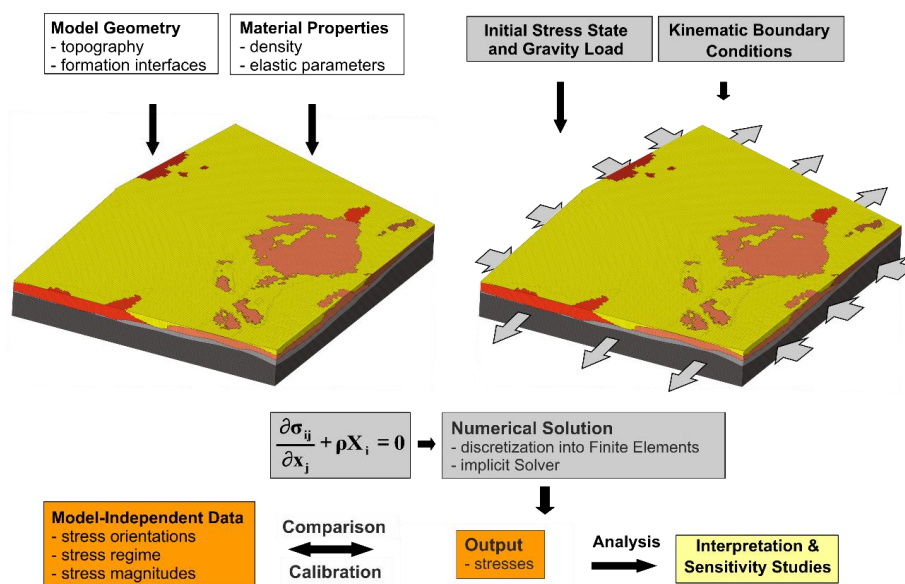
**Figure 3: General workflow of 3D geomechanical-numerical modelling. White boxes: Assembly of model geometry and rock properties. Left figure: 3D view of the discretized model volume. Grey boxes: Initial stress field and kinematic boundary**
155    **conditions, gravity load and numerical solution. An appropriate initial stress state and kinematic boundary conditions are determined and applied as well as gravity load. Right figure: Discretized model volume including boundary conditions used. The partial differential equation of the equilibrium of forces in 3D is solved using the FEM ($\sigma_{ij}$ stress tensor, $x_j$ Cartesian coordinates, $\rho$ density, and $X_i$ body forces). Orange boxes: Model results are calibrated against model-independent observations. Yellow box: Once the fit to the model-independent observations is acceptable, i.e. within their uncertainties, an interpretation and analysis of**
160    **the model results can be performed.**

### 3.2 Model geometry

The model geometry extends over 1250 km in east-west direction from eastern Poland to western France and by 1000 km in north-south direction from southern Scandinavia to northern Italy covering an area of about 1.25 million km². This area was chosen with regard to the orientation of $S_{Hmax}$ to simplify the definition of boundary conditions later on and with regard to

165    important crustal structures which may affect the recent stress field in Germany, e.g. the Bohemian Massif, the Tornquist Suture and the European Cenozoic Rift System. Additionally, model boundaries are selected distal to the German border to avoid possible boundary effects in the area of main interest. (Fig. 1)

The model geometry contains four major units: A sedimentary cover, the upper crust, the lower crust and parts of the lithospheric mantle. The units are bounded by five surfaces: The topography, the top of the crystalline basement, the top of

170    the lower crust, the Mohorovičić discontinuity (Moho) and the model base at 100 km depth. The bottom of the model is thus

not defined as the LAB and therefore the thickness of the lithospheric mantle can deviate from its real thickness. The Moho was chosen as the deepest surface since almost all calibration data are from above and also the depth interval of greatest interest are the upper 10 km of the crust. Although deeper structures may exert a long-wavelength effect on the stress state in the upper crust we expect that the primary contributions to the stress field are captured by the considered interfaces. The

175    upper crust is laterally sub-divided into four parts: The East European Craton, Avalonia, the Armorican Terrane Assemblage and the ALCAPA unit referring to the tectonic units displayed in Fig. 1c.
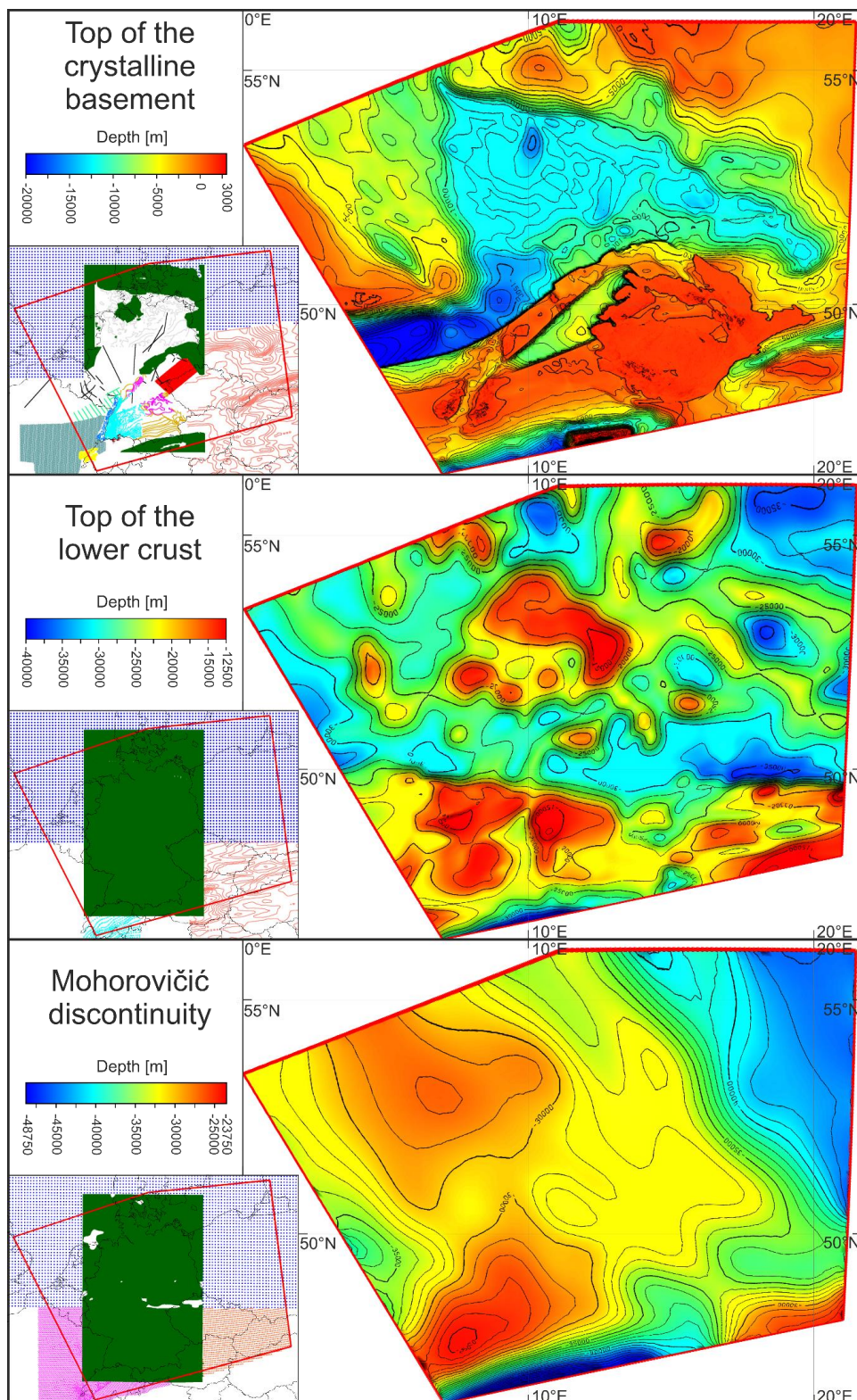
**Figure 4: Database and depth maps of the top of the crystalline basement, the top of the lower crust and the Mohorovičić**
**discontinuity. Used data are: Crystalline basement: Anikiev et al., 2019 (dark green), Diebold et al., 1991 (brown), GeORG-**
180 **Projektteam, 2013 (light blue), Geothermieatlas Bayern, 2004 (pink), Hurtig et al., 1992 (blue green), Kirsch et al., 2017 (red),**
**Korsch and Schäfer, 1995 (light green), Lindner et al., 2004 (grey), Maystrenko and Scheck-Wenderoth, 2013 (dark blue),**
**Reinhold, 2005 (orange), Rupf and Nitsch, 2008 (cyan), Sommaruga, 1999 (yellow), Tašárová et al., 2016 (light red), black profiles**
**(Behr et al., 1994; Bokelmann and Bianchi, 2018; Janik et al., 2011; Cazes et al., 1985; Freeman, 1992; Grad et al., 2009a;**
**Heinrichs et al., 1994; Hirschmann, 1996; Oncken et al., 2000; Schintgen, 2015; Reinhold, 2005; Wenzel and Brun, 1991; Bormann**
185 **et al., 1986; Kirsch et al., 2017; Meschede and Warr, 2019). Top of the lower crust: Anikiev et al., 2019 (dark green), Maystrenko**
**and Scheck-Wenderoth, 2013 (dark blue), Tašárová et al., 2016 (light red), Valasek and Mueller, 1997 (cyan). Mohorovičić**
**discontinuity: Anikiev et al., 2019 (dark green), Grad et al., 2009b (red); Maystrenko and Scheck-Wenderoth, 2013 (dark blue);**
**Wagner et al., 2012 (pink).**

190    Figure 4 shows the depth maps of the top crystalline basement, the top of the lower crust and the Moho with the

corresponding database used. The model is mainly based on three existing models. The 3D Deutschland model (Anikiev et

al., 2019) the Central European Basin model (Maystrenko and Scheck-Wenderoth, 2013) and the Central Europe model of

Tašárová et al. (2016).

The key challenge was the construction of the top crystalline basement. In all the models used and also in most other datasets

195    the base of the sedimentary layer is defined as the top of the basement regardless of whether the basement consists of

crystalline or low-grade metamorphic rocks. This is an assumption which is not sufficient to represent the stiffness contrast

correctly. The main reason for this assumption is the lack of data due to the usually great depths and the lack of economic

interest in these units. Especially in the Rhenohercynian and Saxothuringian Zone (Fig. 1c) only a few seismic profiles exist

from research projects like DEKORP (Meissner and Bortfeld, 1990), EGT (Freeman, 1992) or ZENTROSEIS (Bormann et

200    al., 1986). Despite the uncertainties due to this poor amount of data, the use of the sediment-crystalline boundary is

necessary for a geomechanical-numerical model, because of the strongly different mechanical properties. An extreme

example within our model area is the western part of the Rhenohercynian Zone. Here the basement is outcropping, e. g. in

the Rhenish Massif, but the top of the crystalline crust is suspected to be at about 20 km depth (Schintgen, 2015; Oncken et

al., 2000). Therefore, in those areas where the definition of the basement does not correlate to the top of the crystalline

205    basement, we constructed this surface to obtain a mechanically uniform surface; data used are shown in Fig. 4. The

boundaries between the Variscan basement units are simplified as vertical.

### 3.3 Model discretization

Our final mesh shown in Fig. 5 comprises 1.32 million hexahedral elements with a lateral homogenous resolution of

approximately $6 \times 6$ km$^2$. The vertical resolution decreases with depths from 800 m near the surface up to 7500 m at the base

210    of the model. An exception is the uppermost element layer, which is only 50 m thin to reduce the impact of free surface

effects in the uppermost units. Due to the complex geometry of our model we decided not to use the common approach in

the upper units in which each unit is meshed individually. Only the mantle and the crust are meshed as whole. Then we use

the tool ApplePy (Ziegler et al., 2019) to assign each finite element to the respective subunits and the appropriate rock

properties.
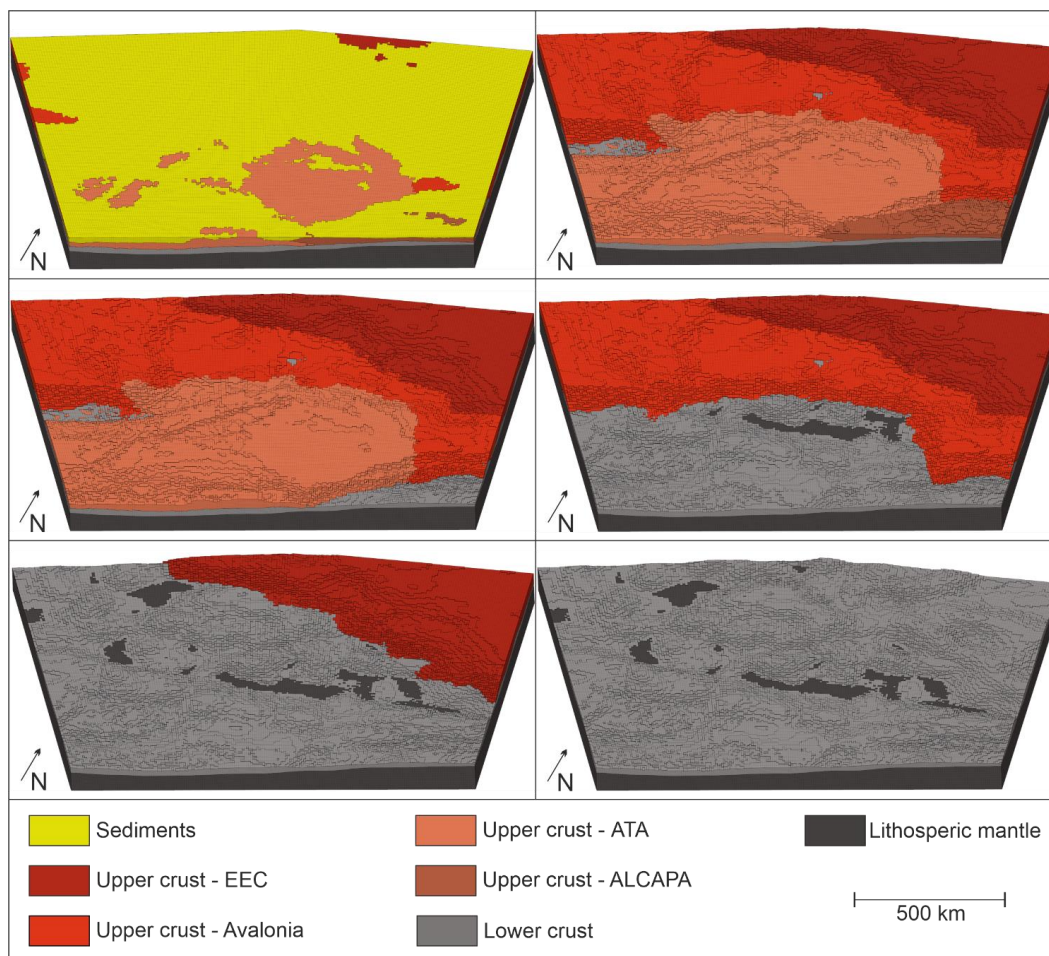
215

**Figure 5: Six different views of the discretized model showing the internal model structure. The sedimentary unit is colored in yellow, the upper crust in different red shades regarding to different tectonic units (Fig. 1c), the lower crust in light grey and the lithospheric mantle in dark grey. The dimension of the model is 1000 x 1250 x 100 km³ comprising 1.32 million hexahedral elements. ATA - Amorican Terrane Assemblage, EEC - East European Craton.**

220

### 3.4 Rock properties

The material properties used in the model and corresponding references are shown in Table 2. The assignment of mean rock properties to the sediment unit is a difficult task, due to the large number of different rock types represented by unconsolidated rocks, claystones, sandstones, salt or limestones. Therefore, the values are approximate mean values. For the

225    upper crust we applied a different density for each tectonic unit in the range of 2750 to 2820 kg m$^{-3}$. The Young's modulus and Poisson's ratio are values for granodiorite as the characteristic rock of the upper crust. For the lower crust density we use the results of Maystrenko and Scheck-Wenderoth (2013) and Tašárová et al. (2016) but since, unlike them, we have only one uniform unit, we use an average of 3000 kg m$^{-3}$. The Young's modulus and the Poisson's ratio are again values for the characteristic rock of the unit, in this case gabbro.

230

Table 2: Overview of the parameters used for the parametrization. [a]Turcotte and Schubert (2014), [b]Maystrenko and Scheck-Wenderoth (2013), [c]Tašárová et al. (2016), [d]Przybycin et al. (2015)

| Unit | Density [kg m⁻³] | Young's modulus [GPa] | Poisson's ratio [-] |
|---|---|---|---|
| Sediments | 2300 | 30 | 0,25 |
| Upper crust | | | |
| ALCAPA | 2750[b] | 70[a] | 0,25[a] |
| Amorican Terrane Assemblage | 2790[c] | 70[a] | 0,25[a] |
| Avalonia | 2820[b] | 70[a] | 0,25[a] |
| East European Craton | 2810[b] | 70[a] | 0,25[a] |
| Lower crust | 3000[b,c] | 80[a] | 0,25[a] |
| Lithospheric mantle | 3300[c,d] | 130 | 0,28[a] |

235

### 3.5 Initial stress state

Before applying displacement boundary conditions to the model an initial stress state is generated representing a reference stress state. We use a simple semi-empirical function by Sheorey (1994), which can be considered as being representative for tectonically inactive regions with low lateral density contrasts. The resulting stress state has to be in equilibrium with gravity
240 and represents the initial stress state, which is subsequently perturbed by applying displacement boundary conditions that impose the tectonic stress. (Buchmann and Connolly, 2007; Hergert and Heidbach, 2011; Reiter and Heidbach, 2014)

### 3.6 Displacement boundary conditions

The base of the model is fixed vertically, lateral movements are allowed and the model surface is free. At the five lateral boundaries of the model displacement boundary conditions are applied perpendicular to these (Fig. 3) to parametrize past
245 and ongoing tectonic kinematics. The orientations of the model boundaries are chosen parallel or perpendicular to the observed $S_{Hmax}$ orientation. The eastern and western lateral model boundaries are aligned parallel and the northern and southern boundaries perpendicular to the $S_{Hmax}$ orientation. Accordingly, extension is applied to the eastern and western boundaries and shortening to the northern and southern ones.

We use a two-stage approach to find a good agreement with the stress orientation and stress magnitude datasets. First a best-
250 fit with respect to the $S_{Hmax}$ orientation is estimated by an appropriate ratio between the extension and shortening applied. In a second step we vary the magnitude of these displacements on the model boundaries while keeping the ratio constant, so that a best-fit with the stress magnitude data is achieved as well. The calibration is mainly based on the $S_{hmin}$ magnitude due to the larger amount of data from the compilation of Morawietz et al. (2020) and the fact that $S_{Hmax}$ magnitudes are often calculated and not measured and therefore less reliable. For the best-fit model a total extension of 465 m in east-west
255 direction and a total shortening of 325 m in north-south direction is applied.

### 4. Results

#### 4.1 Orientation of the maximum horizontal stress ($S_{Hmax}$)

We compare our model results with the stress orientation (WSM quality A to C) from the WSM database (Heidbach et al., 2018) and some additional data by Levi et al. (2019) from western Austria (Fig. 1a). However, we do not use individual data
260 records for this comparison, but a mean $S_{Hmax}$ orientation is used on a regular 0.5° grid. Using a mean $S_{Hmax}$ orientation avoids effects of data clustering which is often the case in the WSM database and it filters the data for a wavelength of the stress pattern that is representative for the resolution of the model. For the estimation of the mean $S_{Hmax}$ values we use the tool stress2grid from Ziegler and Heidbach (2017). The $S_{Hmax}$ data records are weighted according to their quality and their

distance to the grid points. Each grid point requires at least ten data points within a fixed search radius of 200 km.

265 Furthermore, we only use mean $S_{Hmax}$ orientations that have a standard deviation <25° using the statistics of bi-polar data (Mardia, 1972). The grid contains a total number of 619 data points. The model results are interpolated linearly on a plane at 5 km depth and then the nearest value to each grid point is chosen for the comparison with the mean WSM data.

Figure 6a displays the $S_{Hmax}$ orientation of the model at 5 km depth, whereas Fig. 6c shows the calculated mean $S_{Hmax}$ orientation of the WSM data within the model area. The modelled $S_{Hmax}$ orientations at the model boundaries are controlled

270 by the assigned boundary conditions, thus the orientations are perpendicular to the northern and southern boundaries and parallel to the eastern and western edges. Within the model area the orientation of $S_{Hmax}$ shows a homogenous pattern with a dominant NNW-SSE orientation which rotates slightly to a north-south orientation at the eastern boundary. Figure 6b visualizes the deviation of the model results from the mean WSM data. Blue indicates regions where the model results are rotated anti-clockwise with respect to the mean WSM data and orange regions with a clockwise rotation. There are three

275 areas with larger deviations. One with primarily clockwise rotation in the area of Belgium. The two other areas, located in the northern and south-western part of the model, including the NGB, the eastern part of the Alps and western part of the Carpathians show an anti-clockwise rotation. Apart from these two areas the dominant color is orange, conterminous with a slight clockwise rotation. This trend is also visible in Fig. 6d where the histogram of the deviation between the mean $S_{Hmax}$ orientation derived from the WSM data and the modelled orientation is shown with a median deviation of 6.9° and a mean

280 deviation, calculated from the absolute differences, of 15.4°.
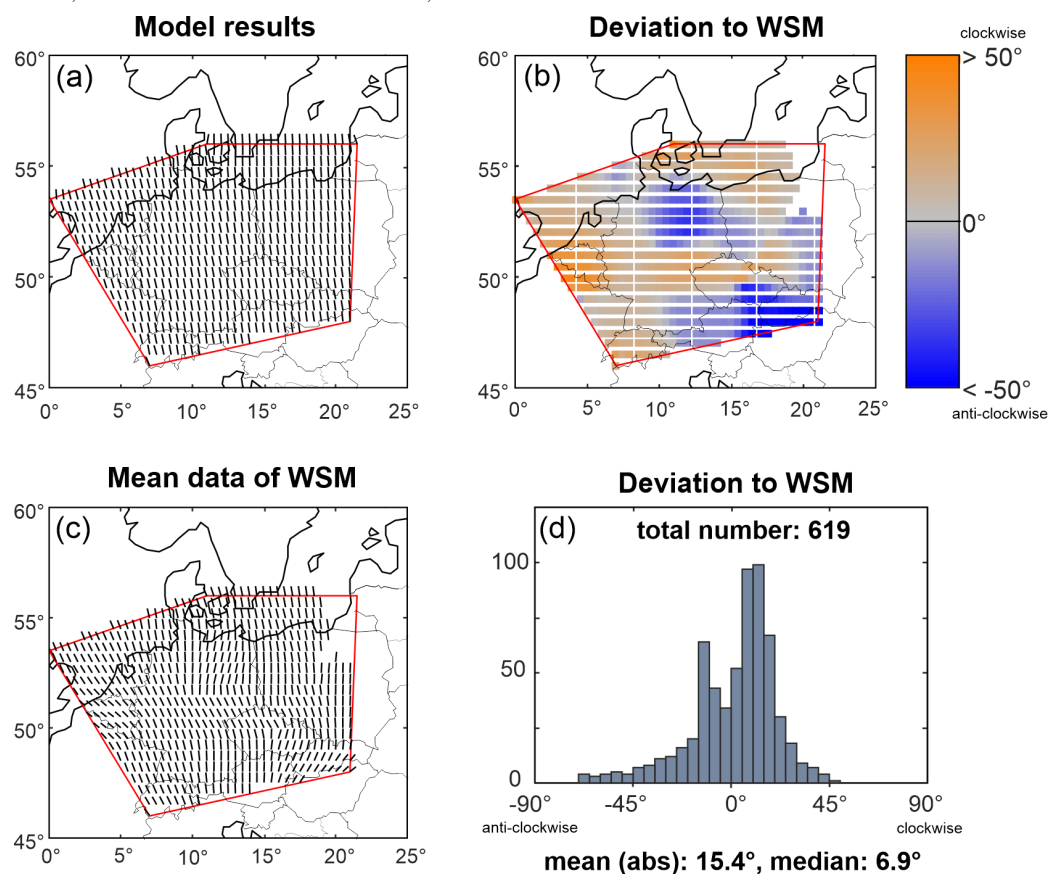
Figure 6: Comparison of $S_{Hmax}$ orientation of the model results with the mean $S_{Hmax}$ orientation derived from WSM data. (a) $S_{Hmax}$ orientation of the model at 5 km depth. (b) Deviation of the model result relative to the mean $S_{Hmax}$ orientation derived from WSM data. (c) Orientation of the mean $S_{Hmax}$ of WSM data (details are described in the text). (d) Histogram of the deviation of the

285 modelled $S_{Hmax}$ orientation to the mean $S_{Hmax}$ orientation derived from WSM data.

### 4.2 Stress magnitudes

### 4.2.1 Minimum horizontal stress ($S_{hmin}$) magnitudes

The modelled magnitudes of $S_{hmin}$ in comparison to stress magnitude data of Morawietz et al. (2020) are shown in Fig. 7. The figure is divided into three subfigures displaying the differences depending on depth and quality (Fig. 7a), the spatial

290   distribution of the calibration data (Fig. 7b) and a histogram showing the distribution of the differences between the modelled and observed $S_{hmin}$ magnitudes (Fig. 7c). The differences are calculated as interpolated model results minus data, thus positive differences correspond to too large model values and negative ones to too low model values. We use only data from Morawietz et al. (2020) with a quality of A, B and C and from depths >200 m, to avoid topographic effects. Thus, we use 74 $S_{hmin}$ magnitude data records from a depth of 200 to 4600 m, most of them from the upper 1000 m. As shown in Fig.

295   7b the data are mainly located within the south-western part with the exception of one measurement from the NGB. With 42 data records, more than half of all data records originate from three localities: From Falkenberg near the German-Czech border (Baumgärtner et al., 1987), from Benken in Switzerland (nagra, 2001) and from Wittelsheim in eastern France (Cornet and Burlet, 1992). Due to the calibration process described in Sect. 3.6 a median difference of 0 MPa is achieved. The differences are, with two exceptions, in a range of -10 to 10 MPa and seem to be independent of depth and quality. This

300   together with a mean difference of 3.3 MPa indicates a very good fit with the data of Morawietz et al. (2020).
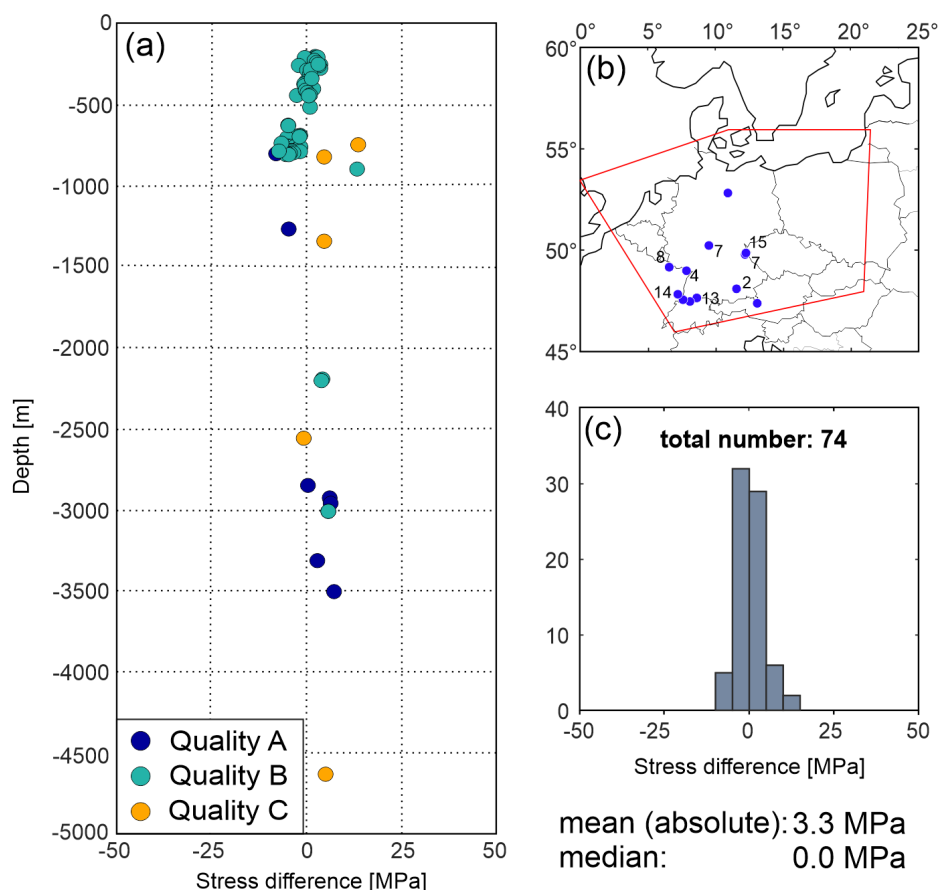
**Figure 7:** $S_{hmin}$ **magnitudes of the model in comparison to the data of Morawietz et al. (2020). The Differences are calculated as model results minus calibration data. (a) Depth depending differences. Color of dots indicate the quality of the calibration data. (b)**
305   **Spatial distribution of the calibration data used, numbers indicating localities with multiple data used. (c) Histogram of the differences displayed in (a).**

### 4.2.2 Maximum horizontal stress ($S_{Hmax}$) magnitudes

For the model calibration regarding the $S_{Hmax}$ magnitudes 57 data records are used from the database of Morawietz et al. (2020). Again, only data with a quality of A to C and from a depth of >200 m are used. Similar to the $S_{hmin}$ data they are

310 mainly located in the south-western part of the model area (Fig. 8b). The data are from seven different localities, whereby the data from Falkenberg near the German-Czech border (Baumgärtner et al., 1987) and from Benken in Switzerland (nagra, 2001) with 25 data records make up almost half of the comparison data used. The mean of the absolute difference is 20.6 MPa and the median difference is 19.3 MPa. This difference can be explained by the asymmetric depth distribution of the values (Fig. 8a). There are significantly more data records from shallower depths (200 to 1000 m) which indicate too large

315 model results than from the greater depths (>1000 m) which indicate too low results. Regardless of this, a trend is visible from positive to negative stress differences with increasing depth, i.e. the model seems to predict too large values of $S_{Hmax}$ in the upper part of the model and too low values of $S_{Hmax}$ in the deeper part. Furthermore, it is striking that the differences of quality A data are almost all negative and almost all of quality B and C are positive.
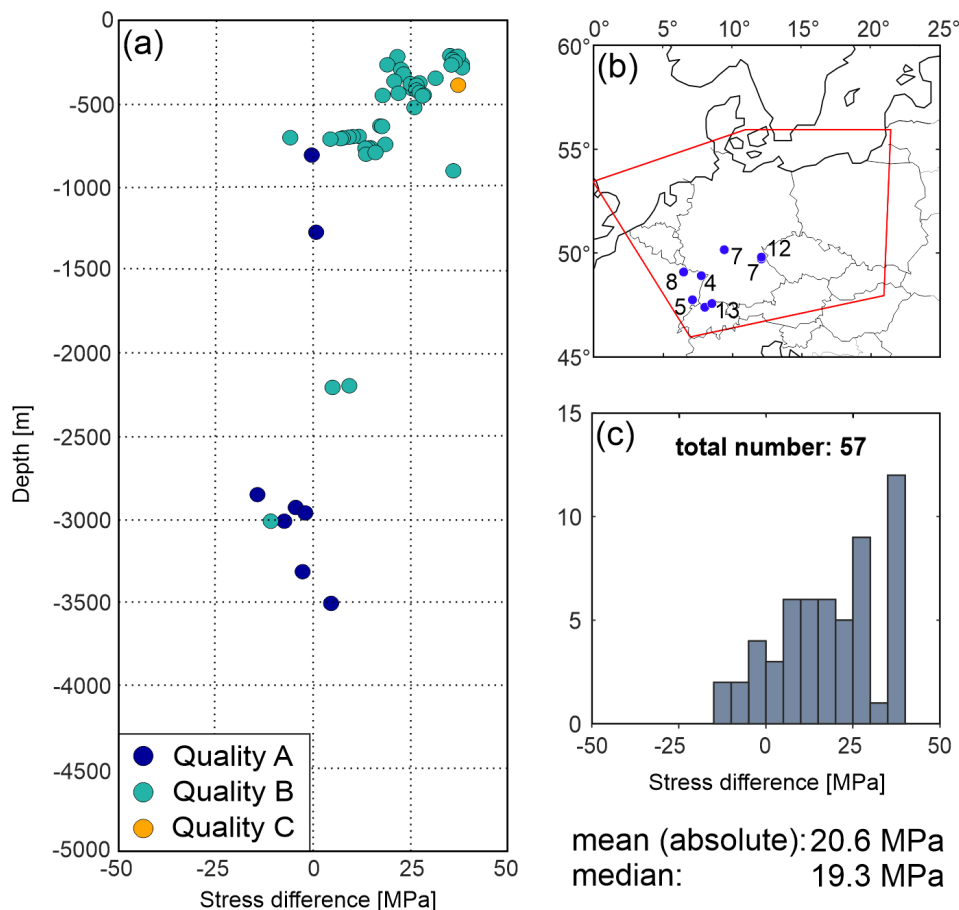
320

**Figure 8: $S_{Hmax}$ magnitudes of the model in comparison to the data of Morawietz et al. (2020). The Differences are calculated as model results minus calibration data. (a) Depth depending differences. Color of dots indicate the quality of the calibration data. (b) Spatial distribution of the calibration data used, numbers indicating localities with multiple data used. (c) Histogram of the differences displayed in (a).**

325

### 4.2.3 Stress gradients and stress regime

Additional to the calibration of the model with stress magnitude data, the absolute stress magnitudes of $S_V$, $S_{hmin}$ and $S_{Hmax}$ for three hypothetical wells up to 10 km depth are shown in Fig. 9. We have chosen these three locations (Fig. 10) due to the availability of stress data for a comparison later on, the quite uniform distribution over Germany (north, south-west and

330 south-east) and the different depths of the crystalline surface. The hypothetic well 1 is entirely within the crystalline basement, well 2 entirely within the sedimentary unit and well 3 partly within the sediment unit and partly within the crystalline basement. As with the previous results we don't show the results of the upper 200 m. The depths are relative to the model surface and do not correspond to the z values of the model.
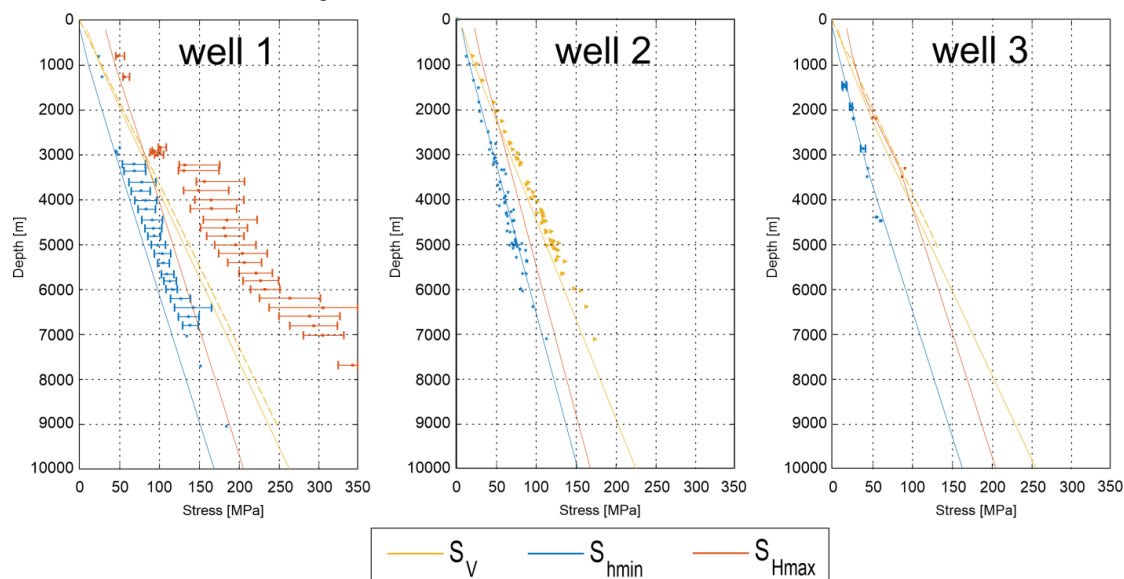
335 **Figure 9: Gradients of $S_V$, $S_{hmin}$ and $S_{Hmax}$ for three hypothetic wells in comparison with data. The colored lines show the stresses of $S_V$ (yellow), $S_{hmin}$ (blue) and $S_{Hmax}$ (red). Blue stars and red rectangles show measured respectively calculated magnitude of $S_{hmin}$ and $S_{Hmax}$. The uncertainties of the magnitudes if specified are displayed as error bars. Yellow dotted lines are calculated $S_V$ from density data. Well 1: Comparison data from the 'Kontinentale Tiefbohrung' (KTB) of Brudy et al. (1997). Well 2: Comparison data from the NGB of Röckel and Lempp (2003). Well 3: Comparison data from Soultz-sous-Forêts and Rittershofen. Measured**
340 **$S_{hmin}$ magnitudes of Valley and Evans (2007), calculated $S_{Hmax}$ values of Klee and Rummel (1993) and calculated $S_V$ magnitudes based on density values of Azzola et al. (2019).**

The $S_V$ gradients of well 1 and 2 are constant with the exception of a slight increase in the upper 1000 m, which is related to free surface effects. Well 3 also shows this effect but with an additional gradient change at 1500 to 3500 m depth. Above 1500 m depth the gradient corresponds to well 2 and below 3500 m to well 1. Overall well 2 shows the lowest $S_V$ gradient of

345 about 22.5 MPa km$^{-1}$, well 1 the highest $S_V$ gradient of about 27 MPa km$^{-1}$ and well 3 is with ~25.5 MPa km$^{-1}$ in between. The horizontal stresses of $S_{hmin}$ and $S_{Hmax}$ have almost constant gradients in well 1 and 2, only the absolute stresses differ. In well 1 we have a gradient of about 17 MPa km$^{-1}$ resulting in 170 MPa at 10km depth for $S_{hmin}$ and about 205 MPa at 10 km for $S_{Hmax}$. Due to the identical gradients the differential stress between $S_{Hmax}$ and $S_{hmin}$ is constant 35 MPa all over the well path. Well 2 show a similar pattern with a $S_{hmin}$ and $S_{Hmax}$ gradient of about 15 MPa km$^{-1}$ and a constant differential stress

350 between $S_{hmin}$ and $S_{Hmax}$ of about 15 MPa. The gradients of well 3 are, as with the $S_V$ magnitudes, a combination of well 1 and 2. This can be seen particularly clearly by the $S_{hmin}$ values of well 3. From the surface to a depth of ~1500 m the gradient is quite similar to well 2 and below ~3500 m to well 1. In between the gradient increases to ~25 MPa km$^{-1}$ which is the highest gradient of all horizontal stresses displayed. As a result, the differential stress in well 3 between $S_{Hmax}$ and $S_{hmin}$ also changes with depth. It amounts to 20 MPa at 1500 m depth, increasing with depth to about 40 MPa at 4000 m and then

355 remains constant leading to 165 MPa for $S_{hmin}$ and 205 MPa for $S_{Hmax}$ at 10 km depth. Well 3 shows thus the only significant

change of horizontal differential stress with depth of all three wells shown and also the highest differential stress with a maximum of about 40 MPa below 4000 m depth.

All three wells show a change of the stress regime from strike-slip to normal faulting, with $S_V$ becoming greater than $S_{Hmax}$. In well 1 the transition is at about 3500 m, in well 2 at about 2500 m and in well 3 at about 4000 m depth. But despite these

360 minor differences in depth, there are almost no differences between the stress regimes.

As an additional result the regime stress ratio (RSR) (Simpson, 1997) for four model sections are shown in Fig. 10. The RSR (Eq. 1) is a unitless value combining the stress regime index n (Eq. 2) of Anderson (1905) and the ratio of stress differences $\phi$ (Eq. 3):

$$RSR = (n + 0.5) + (-1)^n(\phi - 0.5) \text{ (Simpson, 1997)} \tag{1}$$

365 $$n = \begin{cases} 0 & S_{hmin} < S_{Hmax} < S_V \\ 1 & S_{hmin} < S_V < S_{Hmax} \\ 2 & S_V < S_{hmin} < S_{Hmax} \end{cases} \text{ (Anderson, 1905)} \tag{2}$$

$$\phi = \frac{(\sigma_2 - \sigma_3)}{(\sigma_1 - \sigma_3)} \text{ (Angelier, 1979)} \tag{3}$$

The resulting value between 0 and 3 is the RSR indicating the stress regime divided into 6 classes from radial extension over extension, transtension, transpression and compression to constriction. The results in Fig. 10 show with the exception of peripheral areas a rather uniform change of the stress regime from strike-slip to normal faulting with increasing depth.

370 Starting with a RSR of 1 to 2 at 1000 m resulting in a RSR of 1 to 0 at 10 km depth. The two sections in between at 2000 and 4000 m show the transition with a dominant RSR of 1 to 1.5 and 1 to 0.5, respectively.
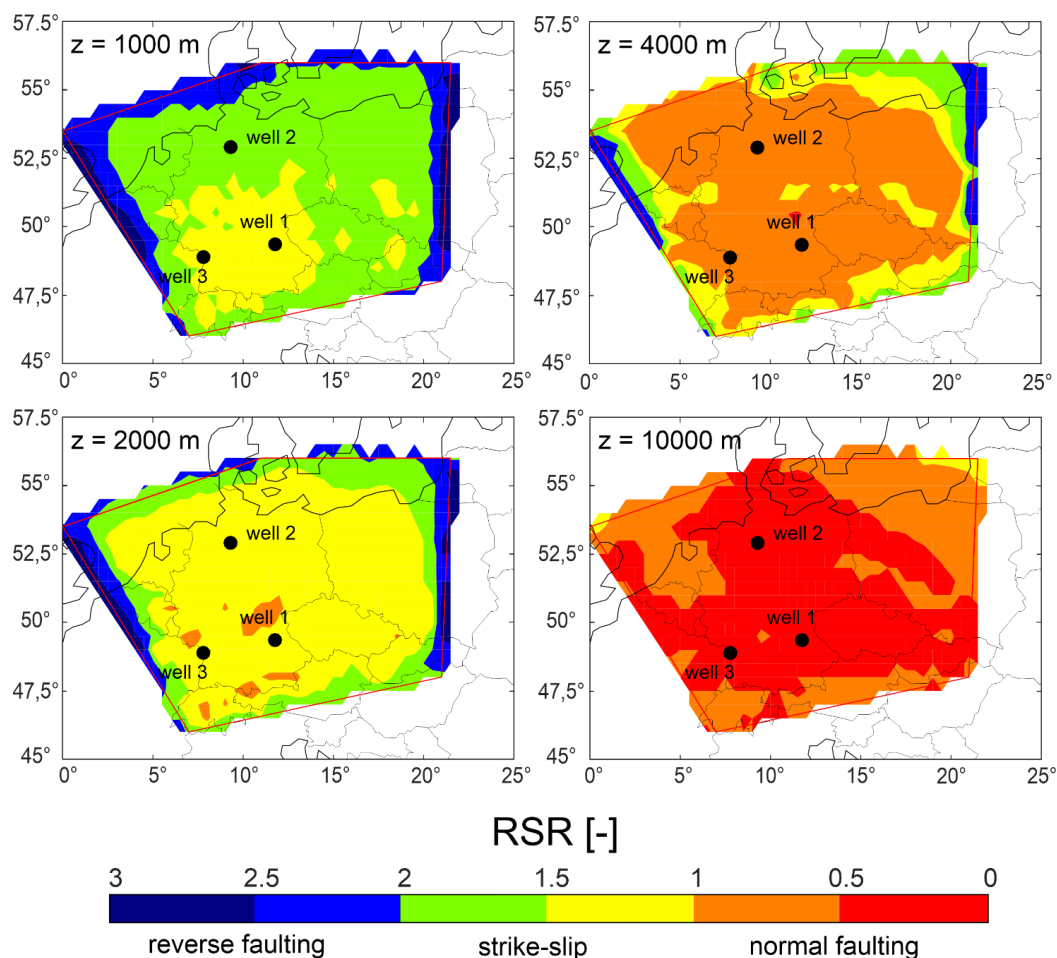
**Figure 10: RSR indicating the stress regime for four model sections for different depths. The three black dots show the locations of the three hypothetical wells in Fig. 9.**

375 **5. Discussion**

**5.1 Orientation of the maximum horizontal stress ($S_{Hmax}$)**

The results of the $S_{Hmax}$ orientation are in comparison to the mean WSM data quite good (Fig. 6). With a median deviation of 6.9° and an absolute mean deviation of 15.4° the results are within the error range of the used WSM A to C quality data records which have uncertainties of 15 to 25° (Heidbach et al., 2018). However, there are three areas with noticeable

380 deviations: In the north-eastern part of Germany, in Belgium and along the Carpathians. The region in north-eastern Germany belongs to the NGB in which there are thick salt deposits. Salt can act as a mechanical decoupling horizon between the layers above and below. In such cases, the stress state below represents the regional trend transferred through the crust while the stress state above is only affected by local sources often controlled by local density and strength contrasts. More than 20 % of the data from this region are above the salt and mostly E-W oriented, in contrast to the data below, which are

385 more N-S oriented (e.g. Heidbach et al., 2007; Roth and Fleckenstein, 2001; Röckel and Lempp, 2003; Grote, 1998; Ahlers et al., 2019). However, since we do not distinguish between the data from these different layers the derived mean $S_{Hmax}$

values are influenced by these data above the salt layer. Possibly the misfit in this area can also be explained by the Pritzwalk anomaly, a positive gravity anomaly due to high-density lower crust (Krawczyk et al., 2008).

The deviations in Belgium and adjacent areas can have several reasons. This region is the border between two massifs, the
390 Rhenish and the Brabant Massif (Pharaoh, 2018), and the strength contrast between these two massifs may play a role. Such contrasts are often considered to be responsible for reorientations in the stress field (e.g. Grünthal and Stromeyer, 1994; Heidbach et al., 2007; Marotta et al., 2004; Reiter, 2020). Another reason could be the tectonically active Lower Rhine Basin nearby or the uplift of the Rhenish Massif (Reicherter et al., 2008). Possible boundary effects can be excluded, since the orientation of $S_{Hmax}$ is uniform along the entire western boundary of the model. The deviations in the south-eastern part of
395 the model are located along the Carpathians and the adjacent Pannonian Basin. This is possibly an area with low far-field horizontal stresses resulting in a near isotropic stress state (Heidbach et al., 2007) and thus the topography contrast between the mountain range and the Pannonian Basin has probably a dominant influence (Bada et al., 2001; 1998). Furthermore, the NE-SW oriented $S_{Hmax}$ indicated by the WSM data implies an NW-SE extension in this area which is in agreement with the orientation of back-arc extension arising from the retreating slab beneath the Carpathians in Romania (Sperner et al., 2001),
400 which the model does not account for.

In general, our modelled $S_{Hmax}$ orientations show a rather simple stress pattern without local perturbations. This is to a certain extent an expectable result since our model is in equilibrium with gravitation. Therefore neither isostatic effects as described by e.g. Kaiser et al. (2005), Bada et al. (2001) or Jarosiński et al. (2006) nor local perturbations due to faults or fault zones (Kaiser et al., 2005; Jarosiński et al., 2006) can be considered since such perturbations are not implemented. Nevertheless,
405 our model results also show no impact of mechanical contrasts on the orientation of $S_{Hmax}$, despite lateral mechanical contrast, e.g. a Young's modulus difference of 40 GPa between the sedimentary (30 GPa) and the upper crustal units (70 GPa).

### 5.2 Magnitudes of $S_{hmin}$, $S_{Hmax}$ and $S_V$

The $S_{hmin}$ magnitudes (Fig. 7a) in general show a very good correlation with the data of Morawietz et al. (2020) independent
410 of data quality and depth. The statistical evaluation supports this with a mean difference of 3.3 MPa, a median difference of 0 MPa and an almost even distribution. However, the model was calibrated with these values, so the almost perfect match should not be overrated.

The comparison of the $S_{Hmax}$ magnitudes does not show such a good match with a mean difference of 20.6 MPa and a median difference of 19.3 MPa (Fig. 8). Due to the calibration process described a much better fit should be achieved. But
415 we have decided not to force a median of 0 MPa for various reasons. Compared to the $S_{hmin}$ magnitude data, the scattering is significantly larger and the distribution is less even. This is an expectable result since $S_{Hmax}$ values are usually calculated and not measured and therefore $S_{Hmax}$ magnitudes have a lower reliability compared to $S_{hmin}$ values (Morawietz et al., 2020) but additionally there seems to be a dependency on depth and quality. A major part of the data indicating too large $S_{Hmax}$ magnitudes are from shallow depths (200 to 1000 m). It can be assumed that the median and mean difference would be
420 significantly better for a uniform depth distribution of the $S_{Hmax}$ values since the results below 1000 m show a good match. A reduction of the $S_{Hmax}$ magnitudes in our model and thus a statistically better fit would therefore only lead to a better fit of the model result in the upper part of the model. Whether there is a dependency of the results on quality is difficult to assess, although data of quality B and C tend to show larger deviations than data of quality A. But most quality B and C data are also from shallow depths. Therefore, the depth dependency may overlay the quality dependency.

425 The stress magnitudes of the three hypothetical wells displayed in Fig. 9 show by and large the expected results. Since $S_V$ is only dependent on the density the gradients of well 1 and well 3 located in a single unit are constant all over the total well depth. The gradient of well 2 changes in between 1500 and 3500 m depth due to the change of the lithological unit. The transition zone is quite large because of the vertical element resolution of about 800 m. Based on the sum of the overburden,

the maximum $S_V$ at 10 km depth is the highest in well 1, followed by well 3 and 2. The stress differences between $S_{Hmax}$ and

430    $S_{hmin}$ are dependent on the elastic rock properties. Therefore, these results again are mainly based on the unit the well is located in. Since the Poisson's ratio is constant for the units involved (0.25) the Young's modulus is probably the decisive parameter. This explains the constant horizontal stress differences within well 1 and 2 and the variations over the length of well 3. In addition, the maximum stress differences seemed to be mainly dependent on the Young's modulus. Well 2 shows the smallest stress differences of 15 MPa and well 1 shows differences of 35 MPa according to a Young's Modulus of 30 and

435    70 GPa, respectively. An exception is well 2 with the highest total stress differences of up to 40 MPa.

To get a more detailed insight we compare our hypothetic wells 1, 2 and 3 with local magnitude data (Fig. 9). The model results of the hypothetic well 1 are displayed in comparison to values of the 'Kontinentale Tiefbohrung' (KTB) a major scientific drilling project in Germany (Brudy et al., 1997). Our results of $S_V$ are in a very good agreement with the $S_V$ calculated from a mean density value. Only at greater depths the difference increases to about 5 MPa and in the uppermost

440    750 m our results are too large, possibly due to free surface effects caused by our model resolution. The results of $S_{hmin}$ and $S_{Hmax}$ show significantly larger differences to the data of Brudy et al. (1997). Except for the values at 3000 m depth the $S_{hmin}$ magnitudes of Brudy et al. (1997) are at least 15 MPa larger than the model results. The maximum difference of about 35 MPa is at 6400 m depth. The results of $S_{Hmax}$ show even greater deviations. All values of Brudy et al. (1997) are at least 15 MPa larger than the model results. The maximum difference is about 180 MPa at 7800 m depth and thus larger than our

445    model results with 160 MPa. Remarkable is the change in the horizontal stress magnitudes of Brudy et al. (1997) at 3000 m depth. The $S_{hmin}$ magnitudes increase from 50 to 70 MPa within 200 m and $S_{Hmax}$ increases even by 30 MPa from 100 to 130 MPa. At the same time the inaccuracies also increase significantly. This can be attributed to the fact that the values between 3000 and 7000 m depth are only calculated and not directly measured (Brudy et al., 1997), which is why the values only got a quality of worse than C (Morawietz et al., 2020) and are not used by us for calibration. A remarkable difference between

450    our model and the geomechanical properties at the KTB site are the values of the Young's modulus. The calculated values of Brudy et al. (1997) are about 90 GPa on average between 3000 and 8000 m depth, which is about 20 MPa larger than our model assumption of 70 GPa in this area. Furthermore, in our model a normal faulting regime is established from about 3500 m depth downwards (Fig. 10), which is contrary to the stress regime of Brudy et al. (1997) showing a strike-slip regime from 1 km depth downwards. This indicate that our $S_{Hmax}$ are possibly too low within this model area. In general, our model

455    results show a constant differential stress between $S_{hmin}$ and $S_{Hmax}$ of 35 MPa whereas the data of the KTB indicate an increasing differential stress with depth. The fact that our model does not include faults can also have an effect. The KTB is located above the Franconian Line and even intersecting it (Wagner et al., 1997). The Franconian Line is a major fault zone at the south-western margin of the Bohemian Massif with a polyphase development from late Paleozoic to Neogene times (Zulauf, 1993; Peterek et al., 1997). In the end it is probably a combination of the lower Young's modulus in the model, the

460    very large uncertainties of the calculated values and too low horizontal stresses in this model region, which may explain the differences of up to 180 MPa for the $S_{Hmax}$ magnitudes.

The stress magnitudes of the hypothetic well 2 are shown in comparison with $S_V$ and $S_{hmin}$ data from the NGB of Röckel and Lempp (2003). The $S_V$ values are in good agreement with our results down to ~2000 m depth, whereas the difference increases below this level. This shows that the density chosen for the sedimentary unit is at least appropriate for the upper

465    part of this unit. A larger density would lead to better results at greater depths but since our calibration data mainly comes from depths shallower than 3500 m (Fig. 7 and 8), we consider assuming a density of 2300 kg m$^{-3}$ for the sedimentary unit is reasonable. The $S_{hmin}$ values indicate a good fit with our results across the entire depth range to 7000 m, which agrees with our general comparison shown in Fig. 7. Due to missing data, a comparison is not possible for the $S_{Hmax}$ values. However, Röckel and Lempp (2003) mention that the actual stress regime in the NGB can be characterized as normal faulting for the

470    sub-salt level. At an average depth of the salt layer in the NGB of 4 km (Scheck-Wenderoth and Lamarche, 2005) our results show a normal faulting regime beneath 4 km depth too (Fig. 10).

For the comparison of our hypothetic well 3 we use data from the geothermal project in Soultz-sous-Forêts and some values from Rittershofen, another geothermal project nearby both located at the western edge of the URG. The URG is part of the major European Cenozoic Rift System located in south-western Germany and eastern France (Ziegler and Dèzes, 2006). The

475 dashed $S_V$ gradients in Fig. 9 are calculated on the base of density values of Rittershofen (Azzola et al., 2019) correlated to the stratigraphic column of Soultz-sous-Forêts based on Aichholzer et al. (2016) up to 5080 m, the total depth of the deepest well in Soultz-sous-Forêts. Despite the density change between the sedimentary unit and the crystalline basement, the $S_V$ magnitudes of the model are in good agreement. An exception are the upper 750 m, where modelled $S_V$ magnitudes are slightly too low. The data of Valley and Evans (2007) show measured $S_{hmin}$ magnitudes between 1500 and 4500 m depth.

480 They are in very good agreement with our model results within the upper 3000 m. In between 3500 and 4500 m depth the agreement is slightly worse but with a maximum difference of about 10 MPa at 4500 m depth still good. For the validation of the $S_{Hmax}$ magnitudes we use four calculated values of Klee and Rummel (1993) between 2200 and 3500 m. Within this depth interval our model results show a good correlation with a maximum deviation of about 5 MPa. Due to the small amount of data available for $S_{Hmax}$, a comparison with some calculated stress gradients can be helpful. Assumptions for stress

485 gradients of Heinemann (1994), Klee and Rummel (1993) and Valley and Evans (2007) result in $S_{Hmax}$ magnitudes of 35 up to 55 MPa at a depth of 2000 m, of 95 up to 143 MPa at 5000 m and of 195 up to 310 MPa at 10 km. Even though these values show a quite wide range, the comparison of the model results allows the conclusion that our $S_{Hmax}$ values show a quite good agreement in the upper 5000 m but tend to be too low with increasing depth. This is also supported by the observation of seismic events which show a slight dominance of strike-slip versus normal faulting focal mechanisms at depths of 8 to 10

490 km in the URG (Cornet et al., 2007). In contrast, our results show a normal faulting regime, which implies to low $S_{Hmax}$ values.

In general, the model results show a good agreement with real magnitude data. The $S_V$ magnitudes show a good correlation for all three described cases of the KTB, the NGB and the Soultz-sous-Forêts site (Fig. 9). The modelled $S_V$ magnitudes appear to be only slightly too low with increasing depth but in general, the densities seem to be quite well chosen. A better

495 agreement would be probably only possible with a higher stratigraphic resolution in the sedimentary unit and a density gradient within the upper crust. Such a simple gradient, which could also reduce the differences in the sedimentary unit, would be in this case less useful, because densities between two sedimentary units can differ considerably, independent of their depth. Overall, the $S_{hmin}$ magnitudes show a very good correlation. This can be seen in the general location-independent comparison in Fig. 7, but also with regard to the Soultz-sous-Forêts and NGB location in Fig. 9. Only the results for the KTB

500 site show some considerable differences, with the greatest deviations from calculated $S_{hmin}$ values (3000 to 7000 m depth) that have not been directly measured and are of rather questionable quality. The $S_{Hmax}$ magnitudes show the largest deviations, both in the general comparison (Fig. 8) and in the local comparisons (Fig. 9). The general comparison shows that our values in the upper part are rather too large and at greater depths rather too small. The results of $S_{Hmax}$ at the KTB and Soultz-sous-Forêts sites only confirm the trend of too low values in the deeper parts, but not the trend of too large values in

505 the shallower parts. In contrast, the $S_{Hmax}$ magnitudes at Soultz-sous-Forêts show a good agreement down to 2000 m depth and the values at the KTB site even indicate too low magnitudes down to 800 m depth. An indication for generally too small values with increasing depth are also the RSR values at 10 km depth (Fig. 10) which show larger areas of values lower than 0.5 indicating a radial extension, an uncommon stress regime in the upper crust. In the upper part of the model up to 4000 m the rather uniform tectonic regime, between normal faulting and transtensional corresponds mainly to the tectonic conditions

510 expected (Röckel and Lempp, 2003; Cornet et al., 2007). However, in detail, e.g. for the KTB site, the model cannot reflect differing local conditions. This could simply be a consequence of the simplifications made, which cannot resolve all local conditions, e.g. differing rock properties or nearby faults.

## 6. Conclusion

The model presented is the first 3D geomechanical model for Western Central Europe predicting the first order 3D stress
515    tensor. The model is calibrated with $S_{Hmax}$ orientations from the WSM database and compilation of $S_{hmin}$ and $S_{Hmax}$ stress
magnitude data from Morawietz et al. (2020). Overall, our model shows good results regarding the orientation of $S_{Hmax}$ and
$S_{hmin}$ magnitudes despite the necessary simplifications due to the model resolution and rock property distributions as well as
the highly irregular spread of the calibration data and their varying quality. The $S_{Hmax}$ orientations of the model are to a large
extend within the uncertainty of the mean $S_{Hmax}$ orientations that are derived from the A to C quality data of the WSM
520    database. Furthermore, the $S_{hmin}$ magnitudes show a quite good fit to various datasets (Röckel and Lempp, 2003; Valley and
Evans, 2007), but the $S_{Hmax}$ magnitudes result show locally significant differences. Modelled $S_{Hmax}$ magnitudes are too small
in the lower part of the model, whereas some results indicate too high values in the upper part. But in general, our model
describes the regional 3D contemporary stress state quite well. Some larger deviations due to local structures are expectable.
Therefore, the model results cannot be used for stress prediction on a local or reservoir scale as the resolution is not
525    sufficient, but it can deliver initial stress conditions for smaller scale models that contain little or no stress magnitude data at
all.

To improve our large-scale model a better stratigraphic resolution of the sedimentary unit and thus a better representation of
the lithologies has to be implemented. This would increase the reliability of the comparison between measured stress
magnitude data and the modelled ones. In addition to a vertical refinement, resolving lateral variations of the rock properties
530    would be useful as well as these potentially account for lateral variability of the stress tensor.

**Author contribution**:

Conceptualization of the project was done by AH, TH, KR, OH and BM. Construction and discretization of the model was
done by SA. Data for the model and its calibration were collected and provided by SA, TH, LR, SM, MS and DA.
535    Evaluation of the model results and their interpretation were performed by SA with the support of AH, TH, KR, BM, LR,
OH and SM. SA wrote the paper with help from all coauthors. All authors read and approved the final paper.

**Competing interests:**

The authors declare that they have no conflict of interest.
540

**Acknowledgments**:

This study is part of the SpannEnD Project (www.SpannEnD-Projekt.de) which is supported by Federal Ministry for
Economic Affairs and Energy (BMWI) and managed by Projektträger Karlsruhe (PTKA) (project code: 02E11637A).
Coastlines and borders used in the figures are based on the Global Self-consistent Hierarchical High-resolution Geography
545    (GSHHG) of Wessel and Smith (1996).

## References

Ahlers, S., Hergert, T., and Henk, A.: Numerical Modelling of Salt-Related Stress Decoupling in Sedimentary
    Basins–Motivated by Observational Data from the North German Basin, Geosciences, 9, 19,
    https://doi.org/10.3390/geosciences9010019, 2019.
550    Aichholzer, C., Duringer, P., Orciani, S., and Genter, A.: New stratigraphic interpretation of the Soultz-sous-
    Forêts 30-year-old geothermal wells calibrated on the recent one from Rittershoffen (Upper Rhine Graben,
    France), Geothermal Energy, 4, 1–26, https://doi.org/10.1186/s40517-016-0055-7, 2016.
Amadei, B. and Stephansson, O.: Rock Stress and Its Measurement, Springer Netherlands, Dordrecht, 490 pp.,
    1997.

555 Anderson, E. M.: The dynamics of faulting, Transactions of the Edinburgh Geological Society, 8, 387–402, https://doi.org/10.1144/transed.8.3.387, 1905.

Andeweg, B.: Cenozoic tectonic evolution of the Iberian Peninsula: Effects and causes of changing stress fields, Ph. D. thesis, Faculty of Earth Sciences, Vrije Universiteit, Amsterdam, 178 pp., 2002.

Angelier, J.: Determination of the mean principal directions of stresses for a given fault population,
560 Tectonophysics, 56, T17-T26, https://doi.org/10.1016/0040-1951(79)90081-7, 1979.

Anikiev, D., Lechel, A., Gomez Dacal, M. L., Bott, J., Cacace, M., and Scheck-Wenderoth, M.: A three-dimensional lithospheric-scale thermal model of Germany, Adv. Geosci., 49, 225–234, https://doi.org/10.5194/adgeo-49-225-2019, 2019.

Asch, K.: The 1:5 Million International Geological Map of Europe and Adjacent Areas (IGME5000),
565 Bundesanstalt für Geowissenschaften und Rohstoffe, 2005.

Azzola, J., Valley, B., Schmittbuhl, J., and Genter, A.: Stress characterization and temporal evolution of borehole failure at the Rittershoffen geothermal project, Solid Earth, 10, 1155–1180, https://doi.org/10.5194/se-10-1155-2019, 2019.

Bada, G., Horváth, F., Cloetingh, S., Coblentz, D. D., and Tóth, T.: Role of topography-induced gravitational
570 stresses in basin inversion: The case study of the Pannonian basin, Tectonics, 20, 343–363, https://doi.org/10.1029/2001TC900001, 2001.

Bada, G., Cloetingh, S., Gerner, P., and Horváth, F.: Sources of recent tectonic stress in the Pannonian region: Inferences from finite element modelling, Geophys. J. Int., 134, 87–101, https://doi.org/10.1046/j.1365-246x.1998.00545.x, 1998.

575 Baumgärtner, J., Rummel, F., and Zhaotan, C.: Wireline hydraulic fracturing stress measurements in the Falkenberg granite massif, Geol. Jb., E 39, 83–99, 1987.

Behr, H. J., Duerbaum, H. J., Bankwitz, P., Bankwitz, E., Benek, R., Berger, H. J., Brause, H., Conrad, W., Foerste, K., Frischbutter, A., Gebrande, H., Giese, P., Goethe, W., Guertler, J., Haenig, D., Haupt, M., Heinrichs, T., Horst, W., Hurtig, E., and Kaempf, H.: Crustal structure of the Saxothuringian Zone; results of
580 the deep seismic profile MVE-90(East), Z. Geol. Wissenschaft., 22, 647–770, 1994.

Bokelmann, G. and Bianchi, I.: Imaging the Variscan suture at the KTB deep drilling site, Germany, Geophys. J. Int., 213, 2138–2146, https://doi.org/10.1093/gji/ggy098, 2018.

Bormann, P., Bankwitz, P., Apitz, E., Bankwitz, E., and Franzke, H. J.: Komplexinterpretation des Profilnetzes ZENTROSEIS - G4 Bericht der SAG Tiefenerkundung - Abschlussbericht, Zentralinstitut für Physik der
585 Erde, Potsdam, 162 pp., 1986.

Brückl, E., Behm, M., Decker, K., Grad, M., Guterch, A., Keller, G. R., and Thybo, H.: Crustal structure and active tectonics in the Eastern Alps, Tectonics, 29, TC2011, https://doi.org/10.1029/2009TC002491, 2010.

Brudy, M., Zoback, M. D., Fuchs, K., Rummel, F., and Baumgärtner, J.: Estimation of the complete stress tensor to 8 km depth in the KTB scientific drill holes: Implications for crustal strength, J. Geophys. Res., 102,
590 18453–18475, https://doi.org/10.1029/96JB02942, 1997.

Buchmann, T. J. and Connolly, P. T.: Contemporary kinematics of the Upper Rhine Graben: A 3D finite element approach, Global Planet. Change, 58, 287–309, https://doi.org/10.1016/j.gloplacha.2007.02.012, 2007.

Cacace, M.: Stress and Strain modelling of the Central European Basin System, Ph. D. thesis, Freie Universität Berlin, Berlin, 167 pp., 2008.

595 Cazes, M., Torreilles, G., Bois, C., Damotte, B., Galdeano, A., Hirn, A., Mascle, A., Matte, P., van Ngoc, P., and Raoult, J. F.: Structure de la croute hercynienne du Nord de la France; premiers resultats du profil ECORS, Bulletin de la Société Géologique de France, I, 925–941, https://doi.org/10.2113/gssgfbull.I.6.925, 1985.

Cornet, F. H. and Burlet, D.: Stress field determinations in France by hydraulic tests in boreholes, J. Geophys. Res.-Sol. Ea., 97, 11829–11849, https://doi.org/10.1029/90JB02638, 1992.

600 Cornet, F. H., Bérard, T., and Bourouis, S.: How close to failure is a granite rock mass at a 5km depth?, Int. J. Rock Mech. Min., 44, 47–66, https://doi.org/10.1016/j.ijrmms.2006.04.008, 2007.

Diebold, P., Naef, H., and Ammann, M.: NTB 90-04: Zur Tektonik der zentralen Nordschweiz - Interpretation aufgrund regionaler Seismik, Oberflächengeologie und Tiefbohrungen, nagra, Wettingen, 277 pp., 1991.

Fischer, K. and Henk, A.: A workflow for building and calibrating 3-D geomechanical models - a case study for a
605 gas reservoir in the North German Basin, Solid Earth, 4, 347–355, https://doi.org/10.5194/se-4-347-2013, 2013.

Franke, W.: The Variscan orogen in Central Europe: Construction and collapse, in: European Lithosphere
Dynamics, edited by: Gee, D. R. and Stephenson, R., Geological Society of London, London, 333–343,
https://doi.org/10.1144/GSL.MEM.2006.032.01.20, 2006.

610 Franke, W.: Tectonostratigraphic units in the Variscan belt of central Europe, GSA Special Papers, 230, 67–90,
https://doi.org/10.1130/SPE230-p67, 1989.

Freeman, R. (Ed.): A continent revealed: The European geotraverse, Cambridge Univ. Pr, Cambridge [u.a.], 275
pp., 1992.

GeORG-Projektteam: Geopotentiale des tieferen Untergrundes im Oberrheingraben: Fachlich-Technischer
615 Abschlussbericht des INTERREG-Projekts GeORG, Teil 4, Freiburg i. Br., 104 pp., 2013.

Geothermieatlas Bayern: Grundgebirge (Prä-Perm) (Verbreitung und Tiefenlage), Bayerisches Staatsministerium
für Wirtschaft, Landesentwicklung und Energie, 2004.

Goelke, M. and Coblentz, D.: Origins of the European regional stress field, Tectonophysics, 266, 11–24, 1996.

Grad, M., Brückl, E., Majdański, M., Behm, M., and Guterch, A.: Crustal structure of the Eastern Alps and their
620 foreland: seismic model beneath the CEL10/Alp04 profile and tectonic implications, Geophys. J. Int., 177,
279–295, https://doi.org/10.1111/j.1365-246X.2008.04074.x, 2009a.

Grad, M., Tiira, T., and ESC Working Group: The Moho depth map of the European Plate, Geophys. J. Int., 176,
279–292, https://doi.org/10.1111/j.1365-246X.2008.03919.x, 2009b.

Grote, R.: Die rezente horizontale Hauptspannungsrichtung im Rotliegenden und Oberkarbon in
625 Norddeutschland, Erdöl-Erdgas-Kohle, 114, 478–483, 1998.

Grünthal, G. and Stromeyer, D.: The recent crustal stress field in Central Europe sensu lato and its quantitative
modelling, Geologie en Mijnbouw, 73, 173–180, 1994.

Heidbach, O., Reinecker, J., Tingay, M., Müller, B., Sperner, B., Fuchs, K., and Wenzel, F.: Plate boundary
forces are not enough: Second- and third-order stress patterns highlighted in the World Stress Map database,
630 Tectonics, 26, TC6014, https://doi.org/10.1029/2007TC002133, 2007.

Heidbach, O., Rajabi, M., Cui, X., Fuchs, K., Müller, B., Reinecker, J., Reiter, K., Tingay, M., Wenzel, F., Xie,
F., Ziegler, M. O., Zoback, M.-L., and Zoback, M.: The World Stress Map database release 2016: Crustal
stress pattern across scales, Tectonophysics, 744, 484–498, https://doi.org/10.1016/j.tecto.2018.07.007, 2018.

Heidbach, O., Tingay, M., Barth, A., Reinecker, J., Kurfeß, D., and Müller, B.: Global crustal stress pattern based
635 on the World Stress Map database release 2008, Tectonophysics, 482, 3–15,
https://doi.org/10.1016/j.tecto.2009.07.023, 2010.

Heinemann, B.: Results of scientific investigations at the HDR test site Soultz-sous-Forêts: Alsace (1987-1992),
SOCOMINE report, 126 pp., 1994.

Heinrichs, T., Giese, P., Bankwitz, P., and Bankwitz, E.: Dekorp 3/MVE-90(West) - preliminary geological
640 interpretation of a deep near-vertical reflection profile between the Rhenish and the Bohemian Massifs,
Germany, Z. Geol. Wissenschaft., 22, 771–801, 1994.

Hergert, T., Heidbach, O., Reiter, K., Giger, S. B., and Marschall, P.: Stress field sensitivity analysis in a
sedimentary sequence of the Alpine foreland, Northern Switzerland, Solid Earth, 6, 533–552,
https://doi.org/10.5194/se-6-533-2015, 2015.

645 Hergert, T. and Heidbach, O.: Geomechanical model of the Marmara Sea region-II. 3-D contemporary
background stress field, Geophys. J. Int., 185, 1090–1102, https://doi.org/10.1111/j.1365-
246X.2011.04992.x, 2011.

Hirschmann, G.: KTB - The structure of a Variscan terrane boundary: seismic investigation - drilling - models,
Tectonophysics, 264, 327–339, https://doi.org/10.1016/S0040-1951(96)00171-0, 1996.

650 Hurtig, E., Cermak, V., Haenel, R., and Zui, V.: Geothermal atlas of Europe, Haack, Gotha (Germany), 156 pp.,
1992.

Jaeger, J. C., Cook, N. G. W., and Zimmerman, R. W.: Fundamentals of rock mechanics, 4. ed., Blackwell Publ,
Malden, MA, 475 pp., 2011.

Janik, T., Grad, M., Guterch, A., Vozár, J., Bielik, M., Vozárova, A., Hegedűs, E., Kovács, C. A., Kovács, I., and
655 Keller, G. R.: Crustal structure of the Western Carpathians and Pannonian Basin: Seismic models from
CELEBRATION 2000 data and geological implications, J. Geodyn., 52, 97–113,
https://doi.org/10.1016/j.jog.2010.12.002, 2011.

Jarosiński, M., Beekman, F., Bada, G., and Cloetingh, S.: Redistribution of recent collision push and ridge push
in Central Europe: insights from FEM modelling, Geophys. J. Int., 167, 860–880,
660 https://doi.org/10.1111/j.1365-246X.2006.02979.x, 2006.

Kaiser, A., Reicherter, K., Huebscher, C., Gajewski, D., Marotta, A. M., and Bayer, U.: Variation of the present-day stress field within the North German Basin; insights from thin shell FE modeling based on residual GPS velocities, Tectonophysics, 397, 55–72, https://doi.org/10.1016/j.tecto.2004.10.009, 2005.

Kirsch, M., Kroner, U., Hallas, P., and Stephan, T.: 3D Model of the Erzgebirge - Crustal-Scale 3D Modelling of the Allochthonous Domain of the Saxo-Thuringian Zone, https://tu-freiberg.de/geo/tectono/3d-erzgebirge, 2017.

Klee, G. and Rummel, F.: Hydrofrac stress data for the European HDR research project test site Soultz-Sous-Forets, Int. J. Rock Mech. Min, 30, 973–976, https://doi.org/10.1016/0148-9062(93)90054-H, 1993.

Kley, J. and Voigt, T.: Late Cretaceous intraplate thrusting in central Europe: Effect of Africa-Iberia-Europe convergence, not Alpine collision, Geology, 36, 839–842, 2008.

Korsch, R. J. and Schäfer, A.: The Permo-Carboniferous Saar-Nahe Basin, south-west Germany and north-east France: basin formation and deformation in a strike-slip regime, Geol. Rundschau, 84, 293–318, https://doi.org/10.1007/BF00260442, 1995.

Kossmat, F.: Gliederung des variszischen Gebirgsbaus, Abh. Sächs. Geol. Landesamtes, 1, 1–39, 1927.

Krawczyk, C. M., Rabbel, W., Willert, S., Hese, F., Götze, H.-J., Gajewski, D., and SPP-Geophysics Group: Crustal structures and properties in the Central European Basin system from geophysical evidence, in: Dynamics of complex intracontinental basins: The Central European basin system, edited by: Littke, R., Bayer, U., Gajewski, D., and Nelskamp, S., Springer, Berlin, Heidelberg, 67–95, 2008.

Kroner, U., Romer, R. L., and Linnemann, U.: The Saxo-Thuringian Zone of the Variscan Orogen as part of Pangea, in: Pre-Mesozoic geology of Saxo-Thuringia: From the Cadomian active margin to the Variscan orogen, edited by: Linnemann, U. and Romer, R. L., Schweizerbart, Stuttgart, 3–16, 2010.

Levi, N., Habermueller, M., Exner, U., Piani, E., Wiesmayr, G., and Decker, K.: The stress field in the frontal part of the Eastern Alps (Austria) from borehole image log data, Tectonophysics, 769, 228175, https://doi.org/10.1016/j.tecto.2019.228175, 2019.

Lindner, H., Scheibe, K., Seidel, K., and Hoffmann, N.: Berechnung von Relief, Tiefenlage und Magnetisierung des magnetisch wirksamen Kristallins für das Norddeutsche Becken, Z. Angew. Geol., 50, 65–74, 2004.

Ljunggren, C., Chang, Y., Janson, T., and Christiansson, R.: An overview of rock stress measurement methods, Int. J. Rock Mech. Min, 40, 975–989, https://doi.org/10.1016/j.ijrmms.2003.07.003, 2003.

Mardia, K. V.: Statistics of Directional Data: Probability and Mathematical Statistics, Academic Press, London, 380 pp., 1972.

Marotta, A. M., Mitrovica, J. X., Sabadini, R., and Milne, G.: Combined effects of tectonics and glacial isostatic adjustment on intraplate deformation in central and northern Europe: Applications to geodetic baseline analyses, J. Geophys. Res., 109, B01413, https://doi.org/10.1029/2002JB002337, 2004.

Marotta, A. M., Bayer, U., Thybo, H., and Scheck, M.: Origin of the regional stress in the North German Basin - results from numerical modelling, Tectonophysics, 360, 245–264, https://doi.org/10.1016/S0040-1951(02)00358-X, 2002.

Maystrenko, Y., Bayer, U., Brink, H.-J., and Littke, R.: The Central European Basin System – an Overview, in: Dynamics of complex intracontinental basins: The Central European basin system, edited by: Littke, R., Bayer, U., Gajewski, D., and Nelskamp, S., Springer, Berlin, Heidelberg, 16–34, https://doi.org/10.1007/978-3-540-85085-4_2, 2008.

Maystrenko, Y. P. and Scheck-Wenderoth, M.: 3D lithosphere-scale density model of the Central European Basin System and adjacent areas, Tectonophysics, 601, 53–77, https://doi.org/10.1016/j.tecto.2013.04.023, 2013.

McCann, T. (Ed.): The Geology of Central Europe Volume 1: Precambrian and Palaeozoic; Volume 2: Mesozoic and Cenozoic, The Geological Society of London, 1449 pp., 2008.

Meissner, R. and Bortfeld, R. K.: DEKORP-Atlas: Results of Deutsches Kontinentales Reflexionsseismisches Programm, Springer Berlin Heidelberg, Berlin, Heidelberg, 21 pp., 1990.

Meschede, M. and Warr, L. N.: The Geology of Germany, Springer, 304 pp., 2019.

Morawietz, S., Heidbach, O., Reiter, K., Ziegler, M., Rajabi, M., Zimmermann, G., Müller, B., and Tingay, M.: An open-access stress magnitude database for Germany and adjacent regions, Geothermal Energy, 8, https://doi.org/10.1186/s40517-020-00178-5, 2020.

nagra: Sondierbohrung Benken: Technical Report NTB 00-01, nagra, 288 pp., 2001.

Oncken, O., Plesch, A., Weber, J., Ricken, W., and Schrader, S.: Passive margin detachment during arc-continent collision (Central European Variscides), in: Orogenic Processes: Quantification and Modelling in the

Variscan Belt, edited by: Franke, W., Haak, V., Oncken, O., and Tanner, D., London, 199–216,
715    https://doi.org/10.1144/GSL.SP.2000.179.01.13, 2000.

Oncken, O.: Transformation of a magmatic arc and an orogenic root during oblique collision and it's
consequences for the evolution of the European Variscides (Mid-German Crystalline Rise), Geol. Rundschau,
86, 2–20, https://doi.org/10.1007/s005310050118, 1997.

Peterek, A., Rauche, H., Schröder, B., Franzke, H.-J., Bankwitz, P., and Bankwitz, E.: The late-and post-Variscan
720    tectonic evolution of the Western Border fault zone of the Bohemian massif (WBZ), Geol. Rundschau, 86,
191–202, https://doi.org/10.1007/s005310050131, 1997.

Pharaoh, T.: The Anglo-Brabant Massif: Persistent but enigmatic palaeo-relief at the heart of western Europe, P.
Geol. Assoc., 129, 278–328, https://doi.org/10.1016/j.pgeola.2018.02.009, 2018.

Przybycin, A. M., Scheck-Wenderoth, M., and Schneider, M.: Assessment of the isostatic state and the load
725    distribution of the European Molasse Basin by means of lithospheric scale 3D structural and 3D gravity
modelling, Int. J. Earth Sci., 104, 1405–1424, 2015.

Reicherter, K., Froitzheim, N., Jarosinski, M., Badura, J., Franzke, H.-J., Hansen, M., Hubscher, C., Müller, R.,
Poprawa, P., Reinecker, J., Stackebrandt, W., Voigt, T., Eynatten, H. von, and Zuchiewicz, W.: Alpine
tectonics north of the Alps, in: The Geology of Central Europe Volume 1: Precambrian and Palaeozoic;
730    Volume 2: Mesozoic and Cenozoic, edited by: McCann, T., The Geological Society of London, 1233–1285,
https://doi.org/10.1144/CEV2P.7, 2008.

Reinhold, K.: Tiefenlage der "Kristallin-Oberfläche" in Deutschland - Abschlussbericht, Bundesanstalt für
Geowissenschaften und Rohstoffe, Hannover, 89 pp., 2005.

Reiter, K. and Heidbach, O.: 3-D geomechanical–numerical model of the contemporary crustal stress state in the
735    Alberta Basin (Canada), Solid Earth, 5, 1123–1149, https://doi.org/10.5194/se-5-1123-2014, 2014.

Reiter, K., Heidbach, O., Reinecker, J., Müller, B., and Röckel, T.: Spannungskarte Deutschland 2015, Erdöl-
Erdgas-Kohle, 131, 437–442, 2015.

Reiter, K.: Stress rotation – The impact and interaction of rock stiffness and faults, Solid Earth Discussions,
https://doi.org/10.5194/se-2020-129, 2020.

740    Reiter, K., Heidbach, O., Müller, B., Reinecker, J., and Röckel, T.: Stress Map Germany 2016,
https://doi.org/10.5880/WSM.Germany2016_en, 2016.

Röckel, T. and Lempp, C.: Der Spannungszustand im Norddeutschen Becken, Erdöl-Erdgas-Kohle, 119, 73–80,
2003.

Roth, F. and Fleckenstein, P.: Stress orientations found in NE Germany differ from the West European trend,
745    Terra Nova, 13, 289–296, https://doi.org/10.1046/j.1365-3121.2001.00357.x, 2001.

Rupf, I. and Nitsch, E.: Das Geologische Landesmodell von Baden-Württemberg: Datengrundlagen, technische
Umsetzung und erste geologische Ergebnisse, Freiburg i. Br., LGRB-Informationen, 21, 81 pp., 2008.

Scheck-Wenderoth, M. and Lamarche, J.: Crustal memory and basin evolution in the Central European Basin
System - new insights from a 3D structural model, Tectonophysics, 397, 143–165,
750    https://doi.org/10.1016/j.tecto.2004.10.007, 2005.

Schintgen, T.: The Geothermal Potential of Luxembourg - Geological and thermal exploration for deep
geothermal reservoirs in Luxembourg and the surroundings, Ph. D. thesis, Universität Potsdam, Potsdam, 313
pp., 2015.

Schmid, S. M., Fügenschuh, B., Kissling, E., and Schuster, R.: Tectonic map and overall architecture of the
755    Alpine orogen, Eclogae Geolog. Helv., 97, 93–117, https://doi.org/10.1007/s00015-004-1113-x, 2004.

Schmitt, D. R., Currie, C. A., and Zhang, L.: Crustal stress determination from boreholes and rock cores:
Fundamental principles, Tectonophysics, 580, 1–26, https://doi.org/10.1016/j.tecto.2012.08.029, 2012.

Sheorey, P. R.: A theory for In Situ stresses in isotropic and transverseley isotropic rock, Int. J. Rock Mech. Min,
31, 23–34, https://doi.org/10.1016/0148-9062(94)92312-4, 1994.

760    Simpson, R. W.: Quantifying Anderson's fault types, J. Geophys. Res., 102, 17909–17919,
https://doi.org/10.1029/97JB01274, 1997.

Smith, W. H. F. and Sandwell, D. T.: Global Sea Floor Topography from Satellite Altimetry and Ship Depth
Soundings, Science, 277, 1956–1962, https://doi.org/10.1126/science.277.5334.1956, 1997.

Sommaruga, A.: Décollement tectonics in the Jura forelandfold-and-thrust belt, Mar. Petrol. Geol., 16, 111–134,
765    https://doi.org/10.1016/S0264-8172(98)00068-3, 1999.

Sperner, B., Lorenz, F., Bonjer, K., Hettel, S., Müller, B., and Wenzel, F.: Slab break-off - abrupt cut or gradual detachment? New insights from the Vrancea Region (SE Carpathians, Romania), Terra Nova, 13, 172–179, https://doi.org/10.1046/j.1365-3121.2001.00335.x, 2001.

Stromeyer, D. and Heidbach, O.: Tecplot 360 Add-on GeoStress, GFZ Data Services, https://doi.org/10.5880/wsm.2017.001, 2017.

770

Tašárová, Z. A., Fullea, J., Bielik, M., and Środa, P.: Lithospheric structure of Central Europe: Puzzle pieces from Pannonian Basin to Trans-European Suture Zone resolved by geophysical-petrological modeling, Tectonics, 35, 722–753, https://doi.org/10.1002/2015TC003935, 2016.

Turcotte, D. L. and Schubert, G.: Geodynamics, 3. ed., Cambridge Univ. Press, Cambridge, 623 pp., 2014.

775 Valasek, P. and Mueller, S.: A 3D tectonic model of the Central Alps based on an integrated interpretation of seismic refraction and NRP 20 reflection data, in: Deep structure of the Swiss alps: results of NRP 20, edited by: Pfiffner, O. A., Lehner, P., Heitzmann, P., Mueller, S., and Steck, A., Birkhauser Verlag, Basel, 302–325, 1997.

Valley, B. and Evans, K. F.: Stress State at Soultz-Sous-Forêts to 5 km Depth from wellbore failure and hydraulic

780 observations, in: Thirty-Second Workshop on Geothermal Reservoir Engineering, 22-24 January 2007, 2007.

Wagner, G. A., Coyle, D. A., Duyster, J., Henjes-Kunst, F., Peterek, A., Schröder, B., Stöckhert, B., Wemmer, K., Zulauf, G., Ahrendt, H., Bischoff, R., Hejl, E., Jacobs, J., Menzel, D., Lal, N., van den haute, P., Vercoutere, C., and Welzel, B.: Post-Variscan thermal and tectonic evolution of the KTB site and its surroundings, J. Geophys. Res., 102, 18221–18232, https://doi.org/10.1029/96JB02565, 1997.

785 Wagner, M., Kissling, E., and Husen, S.: Combining controlled-source seismology and local earthquake tomography to derive a 3-D crustal model of the western Alpine region, Geophys J Int, 191, 789–802, https://doi.org/10.1111/j.1365-246X.2012.05655.x, 2012.

Wenzel, F. and Brun, J. P.: A deep reflection seismic line across the Northern Rhine Graben, Earth and Planetary Science Letters, 104, 140–150, https://doi.org/10.1016/0012-821X(91)90200-2, 1991.

790 Wessel, P. and Smith, W. H. F.: A global, self-consistent, hierarchical, high-resolution shoreline database, J. Geophys. Res., 101, 8741–8743, https://doi.org/10.1029/96JB00104, 1996.

Ziegler, M. O. and Heidbach, O.: The 3D stress state from geomechanical–numerical modelling and its uncertainties: a case study in the Bavarian Molasse Basin, Geothermal Energy, 8, 65, https://doi.org/10.1186/s40517-020-00162-z, 2020.

795 Ziegler, M. O. and Heidbach, O.: Matlab Script Stress2Grid (Version 1.1), https://doi.org/10.5880/wsm.2017.002, available at: https://github.com/MorZieg/Stress2Grid, 2017.

Ziegler, M. O., Ziebarth, M., and Reiter, K.: Python Script Apple PY v1.0, GFZ Data Services, https://doi.org/10.5880/wsm.2019.001, 2019.

Ziegler, M. O., Heidbach, O., Reinecker, J., Przybycin, A. M., and Scheck-Wenderoth, M.: A multi-stage 3-D

800 stress field modelling approach exemplified in the Bavarian Molasse Basin, Solid Earth, 7, 1365–1382, https://doi.org/10.5194/se-7-1365-2016, 2016.

Ziegler, P. A. and Dèzes, P.: Crustal evolution of Western and Central Europe, Geological Society, London, Memoirs, 32, 43–56, https://doi.org/10.1144/GSL.MEM.2006.032.01.03, 2006.

Zoback, M. L.: First- and second-order patterns of stress in the lithosphere: The World Stress Map Project, J.

805 Geophys. Res.-Sol. Ea., 97, 11703–11728, https://doi.org/10.1029/92JB00132, 1992.

Zulauf, G.: Brittle deformation events at the western border of the Bohemian Massif (Germany), Geol Rundsch, 82, 489–504, https://doi.org/10.1007/BF00212412, 1993.